Continuum dynamic traffic models with novel local route-choice strategies for urban cities

Chengyuan Wu[1], Liangze Yang[2], Jie Du[*3,4,5], Xin Pei[6] and S.C. Wong[7]

[1]*Department of Mathematical Sciences, Tsinghua University, Beijing, 100084, China.*
[2]*School of Mathematical Sciences, Anhui University, Hefei, Anhui, 230601, China.*
[3]*School of Mathematical Sciences, East China Normal University, Shanghai 200241, China.*
[4]*Shanghai Key Laboratory of PMMP, East China Normal University, Shanghai 200241, China.*
[5]*Key Laboratory of MEA, Ministry of Education, China.*
[6]*Department of Automation, BNRIST, Tsinghua University, Beijing, 100084, China.*
[7]*Department of Civil Engineering, The University of Hong Kong, Hong Kong SAR, China.*

Abstract: In dynamic traffic assignment problems, travelers choose routes that minimize their cost of traveling to their destination. In traditional continuum models, travelers have a global perception of traffic; in this study, two novel reactive route-choice strategies are devised in which travelers have a local perception of traffic. In Strategy A, travelers identify a set of feasible temporary destinations that are equidistant from their final destination, and then choose an optimal path within the local perception region that minimizes their cost of traveling to the temporary destination set. In Strategy B, travelers identify a direct path that they can follow to move closer to their final destination within a short, fixed time. These route-choice strategies are used to formulate complete continuum dynamic models for traffic flows in an urban city that consist of a conservation law and a set of eikonal equations or optimization problems involving ordinary differential equations. High-order numerical schemes and suitable solution algorithms are applied to solve these equations on unstructured triangular meshes. Numerical examples are also presented to compare the novel local route-choice strategies with traditional global strategies.

Keywords: continuum modeling, local perception, route-choice strategy, dynamic traffic assignment

1 Introduction

For decades, the solution of traffic flow problems has been crucial to the development of society. Dynamic traffic assignment (DTA) [4, 29] can be applied to many traffic flow problems, such as dynamic traffic management and control, that cannot be simulated by traffic flow models of static scenarios, and can capture many traffic flow features such as shock waves, expansion waves, and

*Corresponding author: jdu@math.ecnu.edu.cn

queue overflows. Consequently, DTA is one of the most active research fields in transportation science.

DTA consists of two components: travel choice and traffic flow. The travel choice principle captures the route-choice strategy of traffic units and directly influences the traffic flow on each road in a study area. The traffic flow principle describes how traffic propagates within a traffic region, which in turn influences travelers' route-choice strategies. These two components of DTA influence each other, and DTA is therefore used to derive a timing-varying flow pattern that satisfies both principles.

Route-choice problems in DTA have been examined in many studies. The dynamic user equilibrium (DUE)-based route-choice strategy [28, 27, 20] is an extension of principle of Wardrop (1952) [47] that assumes that if any two travelers have the same departure time, origin and destination, their travel costs should be equal and minimal. DUE problems can be further categorized into reactive dynamic user equilibrium (RDUE) problems [2, 24, 21] and predictive dynamic user equilibrium (PDUE) problems [28, 27, 13, 14]. In RDUE problems, travelers select the route that minimizes the instantaneous travel cost, adjusting their choices reactively. In PDUE problems, travelers are assumed to possess perfect information about the modeled domain, allowing them to choose the route that minimizes the actual travel cost in a predictive manner. Moreover, a stochastic extension of the DUE principle has been developed: the stochastic dynamic user equilibrium (SDUE)-based route-choice strategy [38, 41]. Some route-choice strategies are non-equilibrium but nevertheless of great significance [36]. The dynamic system optimal (DSO)-based route-choice strategy [32, 33] assumes that travelers cooperate when choosing a path and aims to minimize the total travel cost of a system over a given period. The bounded rational (BR) model [12] assumes that travelers have a limited ability to consider all possible routes and thus heuristically identify a small subset of routes, from which they choose the best route.

People often use heuristic rules when making decisions, which leads to bias and systematic errors [10]. For example, BR problems can arise due to cognitive limits and deliberation costs in route choices [16], violation of the shortest-path principle [1, 37], and nonexistence of perfect rationality via learning processes [10, 31, 16]. As such, the route-choice strategy used by Xia et al. [51] is based on a traffic-cost function that is influenced by travelers' memory and current traveler densities, whereas that used by Hoogendoorn et al. [19] is based on computing a local potential function to determine how to avoid high-density areas.

Two different modeling approaches are used to examine DTA problems: the discrete modeling approach and the continuum modeling approach. The discrete modeling approach is used for detailed examination of travel patterns in road network systems. In contrast, the continuum modeling approach—which we employ in the current study—is used to examine the overall behavior of travelers at a macroscopic level, as its treatment of the modeled region and its dense network as a continuum allows certain characteristics, such as the traffic flow intensity and density, to be represented by smooth mathematical functions [44]. The first continuum model to be devised was the Lighthill–Whitham–Richards (LWR) model [26, 39], which deals with a one-dimensional scenario. The LWR model has since been extended to two-dimensional models of highly dense transportation systems [3, 49, 48, 17, 18, 54]. Huang et al. [21] followed the route-choice strategy provided in [49] by developing a continuum RDUE model that consists of a conservation law that governs the traffic flow and an eikonal equation that represents the instantaneous traffic cost. Du et al. [13] constructed a PDUE-based route-choice strategy and a DTA model that consists of a conservation law and the Hamilton–Jacobian equation, which identify the real travel cost. Du et al. [14] further extended their earlier model to apply to anisotropic scenarios. Long et al. [30] devised a two-level

continuum transportation system approach to modeling a dynamic taxi traffic-assignment problem using real-time traffic information. Yang et al. [52] formulated a continuum model of air pollution based on traffic flow as a coupled system comprising a conservation law, an eikonal equation, and an advection–diffusion equation.

The majority of aforementioned continuum DTA models assume that travelers possess a global perspective when selecting a route. This assumption is valid when travelers have full knowledge of the global dynamic distributions of all other travelers; such knowledgeable travelers are those in, for example, automated vehicles or those with navigation systems connected to intelligent traffic systems. When drivers of cars with navigation systems are unfamiliar with an area, they usually follow the shortest route suggested by these systems. However, many traditional travelers have only a local perspective of traffic dynamics, such as commuters in small or medium-sized cities. These travelers generally consider only local traffic information, such as information obtained from what they can see or from radio broadcasts, and thus make route choices based on their own judgment of local traffic conditions. They may also use intelligent maps to obtain local information (e.g., traffic density) to assist them to drive around their local area.

Nevertheless, although it is possible for drivers to obtain full real-time information about their destination from radio broadcasts and intelligent maps, some drivers only consider local information and ignore information about remote places, as traffic conditions change dynamically and local information is relatively more important. Furthermore, humans have a limited ability to consider global information; thus, drivers usually preset their intelligent map or navigation device to have a certain visibility window around their location, and thus the map or device shows only the traffic conditions within this window. Drivers therefore have their own local field of perception that is determined by various factors, such as the road intersection width, the block size, and the setting of their navigation device. In this case, the traditional assumption that drivers have a global perspective does not hold, and therefore drivers' route-choice strategies must be reformulated from a local perspective. The objective of this paper is to develop mathematical models and corresponding numerical methods that accurately represent real-life scenarios.

Research on local route-choice problems has mainly focused on pedestrian flows determined from local visual information. However, local route-choice problems can also be applied to traffic flow problems, and most local route-choice studies have used a microscopic-level discrete modeling approach. For example, Guo and Huang [15], Zeng et al. [53], and Wang et al. [46] have divided a global region into several smaller shapes representing the local views of pedestrians based on pedestrians' experience. Zhou et al. [58] considered that pedestrians set various temporary target exits during their journeys. Hoogendoorn et al. [19] developed a model consisting of local route-choice strategies that avoided high-density areas, but although this model is continuous, unlike discrete models it does not explicitly consider the concept of a local view.

Accordingly, in this study, we use a continuum modeling approach to consider a DTA problem in a city. We assume that there is only one type of vehicle and focus on the construction of local route-choice strategies, which allows us to study the behavior of travelers with a local and reactive perspective of traffic dynamics. Based on these strategies, we construct several route-choice models that are applicable to real-life traffic scenarios, and inspired by discrete models, we devise two precise local route-choice strategies: Strategy A and Strategy B. In Strategy A, travelers first identify feasible temporary destinations that are equidistant from their final destination and then determine an optimal path within their local perception region such that a local RDUE principle is satisfied. The DTA model for Strategy A consists of a conservation law to describe the traffic flow and a locally defined eikonal equation to determine the travel choice. In Strategy B, travelers

directly compute their path within their local region, so that they can move close to their final destination within a short time. The complete model for Strategy B consists of a conservation law, an ordinary differential equation (ODE), and an optimization problem. We provide detailed solution procedures for these models, give numerical examples to demonstrate the validity of the model and the solution algorithms, and compare the new local strategies with two traditional global route-choice strategies.

As in some traditional continuum traffic flow models, the conservation law plays an important role in our new models and requires a suitable numerical scheme. In [21], the Lax–Friedrichs scheme was used. However, the scheme is only first-order accurate. In [22, 59], finite-difference (FD) high-order weighted essentially non-oscillatory (WENO) methods on rectangular meshes were applied. However, FD WENO schemes require large computational stencils and are difficult to extend to unstructured meshes. In computational fluid dynamics applications, the discontinuous Galerkin (DG) methods [7, 6, 5, 8, 9] have demonstrated good stability, high orders of accuracy, h–p adaptivity, and flexibility for solving complex geometry problems; however, they have rarely been applied for solving traffic flow problems. In this paper, we adopt a high-order DG method to solve the conservation law. Compared with the FD WENO scheme, the DG method requires a highly compact computational stencil and hence is more suitable for the treatment of different boundary conditions and parallel coding. We also add a high-order WENO limiter [60, 57] to the DG method to avoid numerical oscillations near strong shocks. Moreover, a high-order positivity-preserving (PP) limiter [55] is added to theoretically avoid a negative nonphysical value of density while maintaining flow conservation. In addition to solving the conservation law, we also need to locally solve eikonal equations or ODE problems in different route-choice strategies. In this paper, we use high-order fast sweeping methods [56, 35, 50] to solve the eikonal equations and adopt high-order nonlinearly stable Runge–Kutta (RK) discretizations [40] to solve the ODE problems. For mesh decomposition, we adopt unstructured triangular meshes, which are suitable for a computational domain with a more general shape and allow for the local refinement of the mesh. These attractive properties are unobtainable using the traditional FD WENO method, which is not suitable for unstructured meshes.

The remainder of this paper is organized as follows. The problem and the continuum model are described in Section 2. Two novel route-choice strategies are detailed in Section 3, together with the complete model formulation. Numerical schemes and algorithms to solve the models are given in Section 4. The numerical results and a comparison of various route-choice strategies are detailed in Section 5. Finally, conclusions and suggestions for further studies are given in Section 6.

2 Problem assumptions and description of the continuum model

This section describes the basic construction of the continuum model. Section 2.1 presents the background to the traffic problem considered in this study and some basic assumptions. Section 2.2 introduces the conservation law that governs the traveler density. Section 2.3 discusses the route-choice strategy to determine the velocity direction used in the conservation law.

2.1 Basic assumptions

In this study, we consider the region modeled by Du et al. [13], which is a city with a single

central business district (*CBD*) and some obstructed areas. As shown in Fig. 2.1, the modeled region is an arbitrary shape, and is denoted as Ω. Let Γ_o be the outer boundary of the city, Γ_c be the boundary of the *CBD*, and Γ_i be the boundaries of the obstructed areas. Thus, $\Gamma := \Gamma_o \bigcup \Gamma_c \bigcup \Gamma_i$ is the boundary of Ω. The trips from travelers' homes to the *CBD* are considered, and we make the following basic assumptions.

- The road network is highly dense and thus the modeled region can be viewed as a two-dimensional continuum. The travelers' homes are continuously located within the modeled region Ω, and travelers depart their homes and travel to the *CBD*.
- The traffic demand varies with time, and as a result, the travelers' departure time choices are known.
- Travelers do not leave the city and are not allowed to enter the obstructed areas, which may be a lake or an undeveloped area. Once travelers have entered the *CBD*, they do not return home within the modeled period $[0, T]$ (in h).
- Travelers are continuously surrounded by a local perception field, which is denoted by the green circle in Fig. 2.2. Travelers only obtain information on traffic within this local field, and use this information to make local route-choice decisions. Figure 2.2 shows a traveler making local decisions during the trip—that is, continually adjusting travel direction based on the local traffic information—and ultimately arriving at the destination.

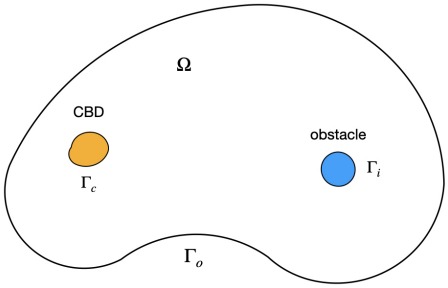

Figure 2.1: **The modeled region.**

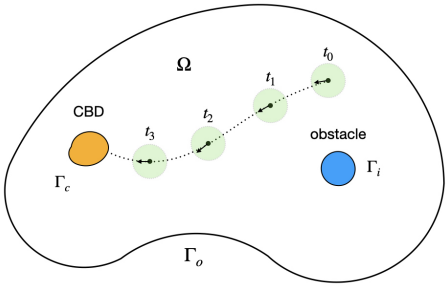

Figure 2.2: **Basic assumption of the local perspective.**

2.2 Conservation laws

We use $\rho(x, y, t)$ (in veh/km^2) and $\mathbf{v}(x, y, t) = (u(x, y, t), v(x, y, t))$ to denote the density and the velocity vector of travelers at location (x, y) at time t, respectively. If the density ρ is known, the norm of the velocity vector $\mathbf{v}(x, y, t)$, i.e., the speed of travelers at location (x, y) at time t, denoted by $U(x, y, t) = ||\mathbf{v}(x, y, t)||$ (in km/h), can be determined. Any given speed density relation can be adopted; in our numerical examples, we use the following Newell's model [34, 11].

$$U = U_f \left\{ 1 - \exp\left[\frac{C}{U_f} \left(1 - \frac{\rho_j}{\rho} \right) \right] \right\}, \qquad \forall (x, y) \in \Omega, \quad t \in [0, T], \tag{2.1}$$

where U_f (in km/h) is the free-flow speed, ρ_j is the jam density, and $C > 0$ (in km/h) is a backward congested wave parameter, i.e., the slope of the fundamental diagram at the given jam density. Here both U_f and ρ_j can vary over space, indicating spatial heterogeneity. Equation (2.1) indicates that speed U decreases as density ρ increases. This model also has the following properties:

$$\begin{aligned} &U \to U_f, \text{ when } \rho \to 0^+ \quad (\text{ when } \rho = 0, \text{ we let } U = U_f)\,; \\ &U = 0, \text{ when } \rho = \rho_j; \text{ and} \\ &Q'|_{\rho=\rho_j} = -C, \text{ when } \rho = \rho_j, \end{aligned}$$

where $Q = U \times \rho$ is the flow variable and $Q\prime = dQ/d\rho$ is the kinematic wave speed. The direction of the velocity vector $\mathbf{v}$ is determined by the route-choice strategy, which is discussed in Section 3.

We use $\mathbf{F}(x, y, t) = \big(f(x, y, t), g(x, y, t)\big)$ to denote the flow vector at location (x, y) at time t, which is defined as

$$\mathbf{F}(x, y, t) = \rho(x, y, t)\mathbf{v}(x, y, t), \quad \forall (x, y) \in \Omega, \quad t \in [0, T]. \tag{2.2}$$

Similar to the mass conservation law in fluid dynamic, $\rho(x, y, t)$ is governed by the following conservation law.

$$\rho_t(x, y, t) + \nabla \cdot \mathbf{F}(x, y, t) = q(x, y, t), \quad \forall (x, y) \in \Omega, \quad t \in [0, T], \tag{2.3}$$

where $q(x, y, t)$ (in $veh/km^2/h$) is the given travel demand at location (x, y) at time t, $\rho_t(x, y, t) = \partial\rho(x, y, t)/\partial t$, and $\nabla \cdot \mathbf{F} = \partial f(x, y, t)/\partial x + \partial g(x, y, t)/\partial y$.

2.3 Review of global route-choice strategies

To determine the density ρ using the conservation law (Eq. (2.3)), we need to determine the direction of the velocity vector $\mathbf{v}$ using the route-choice strategy. In this subsection, we review some global route-choice strategies. It is necessary to define the travel cost first and then choose the travel direction that minimizes this cost.

We use $c(x, y, t)$ (in $\$/km$) to denote the local travel cost per unit distance of travel at location (x, y) at time t, which depends on the local traffic conditions and the preferences of travelers, such as travel time and ambient comfort. Following Du et al. [13, 14], the local travel cost can be computed by

$$c(x, y, t) = \kappa \left(\frac{1}{U(x, y, t)} + \pi(\rho(x, y, t)) \right), \ \forall (x, y) \in \Omega, \ t \in [0, T], \tag{2.4}$$

where κ is the time value, $\frac{\kappa}{U(x,y,t)}$ represents the travel time cost, and $\kappa\pi(\rho(x,y,t))$ represents other density-related expenses.

In continuum RDUE models, travelers choose the route that minimizes the instantaneous total travel cost and change their path in a reactive manner. According to [21], the instantaneous total travel cost from (x,y) to the *CBD* at any fixed time $t \in [0,T]$, denoted $\phi(x,y,t)$, can be computed by solving the following static eikonal equation with suitable boundary conditions:

$$\|\nabla\phi(x,y,t)\| = c(x,y,t), \quad \forall (x,y) \in \Omega, \tag{2.5}$$

where $\nabla\phi(x,y,t) = (\frac{\partial\phi(x,y,t)}{\partial x}, \frac{\partial\phi(x,y,t)}{\partial y})$.

As in continuum PDUE models, travelers consider the actual travel cost and choose a path in a predictive way. Thus, as in [13, 14], the total travel cost incurred by a traveler who departs from location (x,y) at time t to travel to the *CBD* using the constructed path-choice strategy, denoted for simplicity as $\phi(x,y,t)$, can be computed by solving the following time-dependent Hamilton-Jacobi equation:

$$\frac{1}{U(x,y,t)}\phi_t(x,y,t) - ||\nabla\phi(x,y,t)|| = -c(x,y,t), \quad \forall (x,y) \in \Omega, \forall t \in [0,T]. \tag{2.6}$$

The route-choice strategy for all of the models mentioned above at a fixed time t satisfies

$$\mathbf{v}(x,y,t) // -\nabla\phi(x,y,t), \quad \forall (x,y) \in \Omega, \tag{2.7}$$

where '//' indicates that the two vectors are parallel.

In the above-mentioned continuum models, it is assumed that the global traffic information in space is shared by every traveler in the city, such that a traveler at any location $(x_0,y_0) \in \Omega$ knows the density $\rho(x,y,t)$ at any point (x,y) in the city. Hence, the speed function $U(x,y,t)$ and the local travel cost $c(x,y,t)$ can be obtained by computing Eq. (2.1) and Eq. (2.4), respectively. Thus, we can obtain the total travel cost function ϕ by solving Eq. (2.5) or Eq. (2.6) globally in space and then choosing the path according to Eq. (2.7).

3 Local route-choice strategies

The previous section briefly describes the existing continuum models in which travelers have a global perception of traffic information. In contrast, we consider the case in which only local traffic information around (x,y) is considered by travelers located at point (x,y). Two new local route-choice strategies used to determine the direction of the velocity vector $\mathbf{v}(x,y,t)$ are introduced in Section 3.1 and Section 3.2, respectively. The DTA model for both cases is also discussed.

3.1 Strategy A

This subsection introduces the first kind of new route-choice strategy, denoted Strategy A. In classical continuum models, global traffic information is known, and thus travelers always directly choose the best route to the *CBD*, which is a static destination. However, if travelers can only obtain information on traffic conditions in their local area, it is difficult for them to perform global and long-term path planning, especially when they are far away from the *CBD*. In this case, it is

convenient to set several temporary destinations that are closer to travelers rather than taking a far-away *CBD* as the static destination. Therefore, based on local perceptions of traffic information, travelers adjust the temporary destinations dynamically until they reach the final destination.

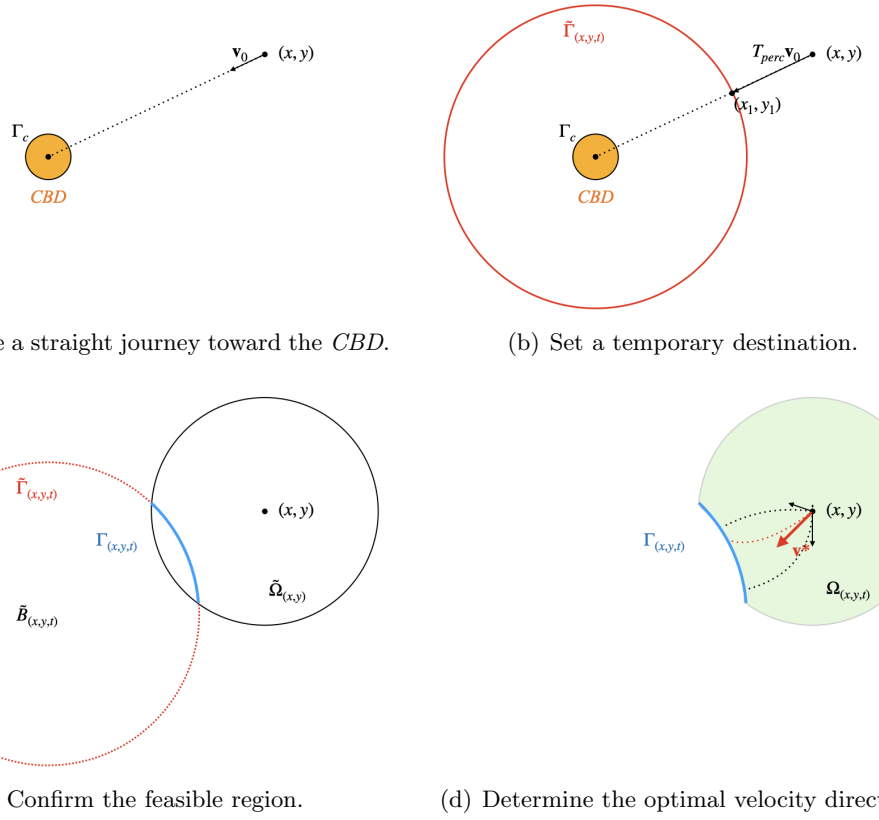

(a) Assume a straight journey toward the *CBD*.

(b) Set a temporary destination.

(c) Confirm the feasible region.

(d) Determine the optimal velocity direction.

Figure 3.1: **Graphical explanation of Strategy A.**

Figure 3.1 illustrates the entire route-choice process for a traveler at a fixed point (x, y) at time t. If travelers do not have much information about traffic conditions, it is reasonable for them to travel directly to the *CBD*. As shown in Fig. 3.1(a), the travel direction $\mathbf{v}_0$ is straight from the current location (x, y) to the center of the final destination *CBD*. A traveler located at (x, y) estimates that after a short time T_{perc} (in s) of traveling along $\mathbf{v}_0$, point (x_1, y_1) will be reached (Fig. 3.1(b)). T_{perc} reflects the traveler's short-term traffic forecasting, which can be described as "predictions made from few seconds to possibly few hours into the future based on current and past traffic information" [45]. In this case, we assume that the location (x_1, y_1) remains located within the local region. Consequently, for our purposes, T_{perc} should not exceed 30 seconds. Additionally, we set T_{perc} to be no less than the look-ahead time $(0.5s - 1.5s)$ of human-driven cars, as described in references [43, 42]. We denote the distance from (x_1, y_1) to the *CBD* center (x_c, y_c) as $d(x, y, t)$. As d is only a preliminary estimate, we treat the speed U as a constant during T_{perc}, as follows:

$$d(x, y, t) = \sqrt{(x_c - x_1)^2 + (y_c - y_1)^2} = \sqrt{(x_c - x)^2 + (y_c - y)^2} - U(x, y, t)T_{perc}.$$

We denote a circle with a center (x_c, y_c) and radius d as $\tilde{\Gamma}(x, y, t)$, which is defined as

$$\tilde{\Gamma}_{(x,y,t)} := \{(x', y') | \sqrt{(x_c - x')^2 + (y_c - y')^2} = d(x, y, t)\}.$$

This is shown as a red circle in Fig. 3.1(b). The circle $\tilde{\Gamma}_{(x,y,t)}$ passes through location (x_1, y_1). Due to traffic congestion, the travel direction $\mathbf{v}_0$ may not be the best choice. All points on the red circle $\tilde{\Gamma}_{(x,y,t)}$ are equivalent temporary destinations, as they are equidistant from the final destination *CBD*. Thus, the traveler determines which path to the circle $\tilde{\Gamma}_{(x,y,t)}$ has the lowest traffic cost.

As shown by the black line in Fig. 3.1(c),we denote a circular region centered at location (x, y) with radius $r_0(x, y, t)$ as $\tilde{\Omega}_{(x,y)}$. The radius $r_0(x, y, t)$ reflects the local perception of travelers and thus may be affected, for example, by the width of a road intersection. We assume that a traveler at point (x, y) can only obtain information on the surrounding traffic conditions within $\tilde{\Omega}_{(x,y)}$. We also assume that the estimation time T_{perc} is not excessively large, i.e., that location (x_1, y_1) remains within the local perception region $\tilde{\Omega}_{(x,y)}$. As shown by the blue line in Fig. 3.1(c), we denote the intersection of $\tilde{\Gamma}$ and $\tilde{\Omega}$ as

$$\Gamma_{(x,y,t)} = \tilde{\Gamma}_{(x,y,t)} \bigcap \tilde{\Omega}_{(x,y)}.$$

$\Gamma_{(x,y,t)}$ therefore contains the feasible temporary destinations within the traveler's local perception domain. Unlike the *CBD* center, which is a point, the blue temporary destination set is an arc. As shown in Fig. 3.1(d), the local computational domain $\Omega_{(x,y,t)}$ marked in green is defined as

$$\Omega_{(x,y,t)} = \tilde{\Omega}_{(x,y)} \backslash (\tilde{\Omega}_{(x,y)} \bigcap \tilde{B}_{(x,y,t)}),$$

where $\tilde{B}_{(x,y,t)}$ is the circular domain bounded by $\tilde{\Gamma}_{(x,y,t)}$. Therefore, the local route-choice problem for a traveler located at point (x, y) at time t can be summarized as follows.

Problem 3.1. *Consider a local computational domain $\Omega_{(x,y,t)}$ with boundary $\Gamma_{(x,y,t)}$, part of which is the temporal destination, as shown in Fig. 3.1(d). Find the optimal travel direction $\mathbf{v}^*(x', y')$ for each point $(x', y') \in \Omega_{(x,y,t)}$ to reach the temporal destination $\Gamma_{(x,y,t)}$, such that an RDUE at time t can be satisfied locally in the region $\Omega_{(x,y,t)}$.*

To solve this problem, we denote the instantaneous travel cost incurred by a traveler who departs from location $(x', y') \in \Omega_{(x,y,t)}$ at time t to travel to temporary destination $\Gamma_{(x,y,t)}$ through the local computational domain $\Omega_{(x,y,t)}$ as $\phi^{loc}_{(x,y,t)}(x', y')$. Unlike in Eq. (2.5) or Eq. (2.6), where the total travel cost function is global and defined for the entire city, the travel cost function $\phi^{loc}_{(x,y,t)}(x', y')$ is defined locally within the circular region $\Omega_{(x,y,t)}$ for a traveler who needs to make a route choice at point (x, y) at time t. Inspired by the continuum model in [21], the route-choice strategy within the local region $\Omega_{(x,y,t)}$ should satisfy

$$\mathbf{v}^*(x', y') // -\nabla \phi^{loc}_{(x,y,t)}(x', y'), \quad \forall (x', y') \in \Omega(x, y, t), \tag{3.1}$$

where $\nabla = (\partial x', \partial y')$. Under the path choice strategy defined in Eq. (3.1) within $\Omega_{(x,y,t)}$, the instantaneous travel cost function $\phi^{loc}_{(x,y,t)}$ can be obtained by solving the following static eikonal equation locally in the domain $\Omega_{(x,y,t)}$:

$$\|\nabla \phi^{loc}_{(x,y,t)}(x', y')\| = c(x', y', t), \quad \forall (x', y') \in \Omega_{(x,y,t)}, \tag{3.2}$$

where c is the local travel cost per unit of distance, which is defined as in Eq. (2.4). The RDUE principle can then be proved as follows.

Theorem 3.1. *If the speed vector $\mathbf{v}^*$ at any fixed location $(x', y') \in \Omega(x, y, t)$ satisfies Eq. (3.1), then the RDUE principle within the local region $\Omega_{(x,y,t)}$ is satisfied.*

Proof. First, let the "used" path p in $\Omega_{(x,y,t)}$ represent the path from origin $O \in \Omega_{(x,y,t)}$ to destination $D \in \Gamma_{(x,y,t)}$ based on the parallel condition defined in Eq. (3.1). Naturally, on some segments of the "unused" path, Eq. (3.1) is not satisfied. The reactive total travel cost C_p along this "used" path is equal to the difference between O and D in terms of $\phi^{loc}_{(x,y,t)}$, in that

$$C_p = \int_p c\ ds \overset{Eq.(3.2)}{=\!=\!=} \int_p \|\nabla \phi^{loc}_{(x,y,t)}\| ds \overset{Eq.(3.1)}{=\!=\!=} -\int_p \nabla \phi^{loc}_{(x,y,t)} \cdot \mathbf{ds} = \phi^{loc}_{(x,y,t)}(O,t) - \phi^{loc}_{(x,y,t)}(D,t).$$

For some regions along any "unused" path $\tilde{p}$ between the same O and D, the parallel condition does not hold, which means that

$$\|\nabla \phi^{loc}_{(x,y,t)}\| ds \geq -\nabla \phi^{loc}_{(x,y,t)} \cdot \mathbf{ds},$$

and thus the travel cost is given by

$$C_{\tilde{p}} = \int_{\tilde{p}} c\ ds \overset{Eq.(3.2)}{=\!=\!=} \int_{\tilde{p}} \|\nabla \phi^{loc}_{(x,y,t)}\| ds \geq -\int_{\tilde{p}} \nabla \phi^{loc}_{(x,y,t)} \cdot \mathbf{ds} = \phi^{loc}_{(x,y,t)}(O,t) - \phi^{loc}_{(x,y,t)}(D,t).$$

This means that the total reactive travel cost along a "used" path is less than that along an "unused" path. This satisfies the user equilibrium conditions in [21], and thus the reactive dynamic user equilibrium (RDUE) holds. □

The route-choice strategy for a traveler at location (x, y) at time t is taken as

$$\mathbf{v}(x,y,t) = \mathbf{v}^*(x,y)// - \nabla \phi^{loc}_{(x,y,t)}(x,y). \tag{3.3}$$

Given that $\|\mathbf{v}\| = U(x,y,t)$ and we can derive the travel direction from Eq. (3.3), we can obtain the following formula for the velocity vector:

$$\mathbf{v}(x,y,t) = -U(x,y,t) \frac{\nabla \phi^{loc}_{(x,y,t)}(x,y)}{\|\nabla \phi^{loc}_{(x,y,t)}(x,y)\|}, \tag{3.4}$$

where $U(x,y,t)$ is the speed function determined by the speed density relation in Eq. (2.1).

In summary, the complete model for Strategy A is constructed as follows:

$$\begin{cases} \rho_t(x,y,t) + \nabla \cdot \mathbf{F}(x,y,t) = q(x,y,t), & \forall (x,y) \in \Omega, \quad t \in [0,T], \\ \mathbf{F}(x,y,t) = \rho(x,y,t)\mathbf{v}(x,y,t), & \forall (x,y) \in \Omega, \quad t \in [0,T], \\ \mathbf{v}(x,y,t) = -U(x,y,t) \dfrac{\nabla \phi^{loc}_{(x,y,t)}(x,y)}{\|\nabla \phi^{loc}_{(x,y,t)}(x,y)\|}, & \forall (x,y) \in \Omega, \quad t \in [0,T], \\ U(x,y,t) = U_f(x,y) e^{-\beta(x,y)\rho^2(x,y,t)}, & \forall (x,y) \in \Omega, \quad t \in [0,T], \end{cases} \tag{3.5}$$

with the following initial boundary conditions

$$\begin{cases} \rho(x,y,0) = \rho_0(x,y), & \forall (x,y) \in \Omega, \\ \mathbf{F}(x,y,t) \cdot \mathbf{n}(x,y) = 0, & \forall (x,y) \in \Gamma_o \cup \Gamma_i, \quad t \in [0,T], \end{cases} \tag{3.6}$$

where the cost function $\phi^{loc}_{(x,y,t)}(x',y')$ can be obtained by solving the following eikonal equation locally for region $(x',y') \in \Omega_{(x,y,t)}$ for each fixed location $(x,y) \in \Omega$ at any fixed time $t \in [0,T]$,

$$\begin{cases} \|\nabla \phi^{loc}_{(x,y,t)}(x',y')\| = c(x',y',t), & \forall (x',y') \in \Omega_{(x,y,t)}, \\ \phi^{loc}_{(x,y,t)}(x',y') = 0, & \forall (x',y') \in \Gamma_{(x,y,t)}. \end{cases} \tag{3.7}$$

The function $\rho_0(x, y)$ in Eqs (3.6) is the given initial density at time $t = 0$. The vector $\mathbf{n}$ is an outward unit normal vector on the boundary $\Gamma_o \cup \Gamma_i$. The second equation in Eqs (3.6) indicates that vehicles do not leave Ω through the outer boundary of the city and are not allowed to enter the obstructed areas. The second equation in Eqs (3.7) is the boundary condition of $\phi^{loc}_{(x,y,t)}(x', y')$, which implies that the instantaneous travel cost decays to 0 when a traveler reaches the feasible temporary destination $\Gamma_{(x,y,t)}$.

Remark 3.1. *It is important to note that even if two distinct locations are in close proximity to one another, their local perception areas differ. Consequently, the travel directions at these locations are determined individually and are likely to vary.*

3.2 Strategy B

Here, we introduce Strategy B, which aims to find a path that allows travelers to directly move closer to the final destination *CBD* in a fixed time T_{perc} (which is as defined in Section 3.1).

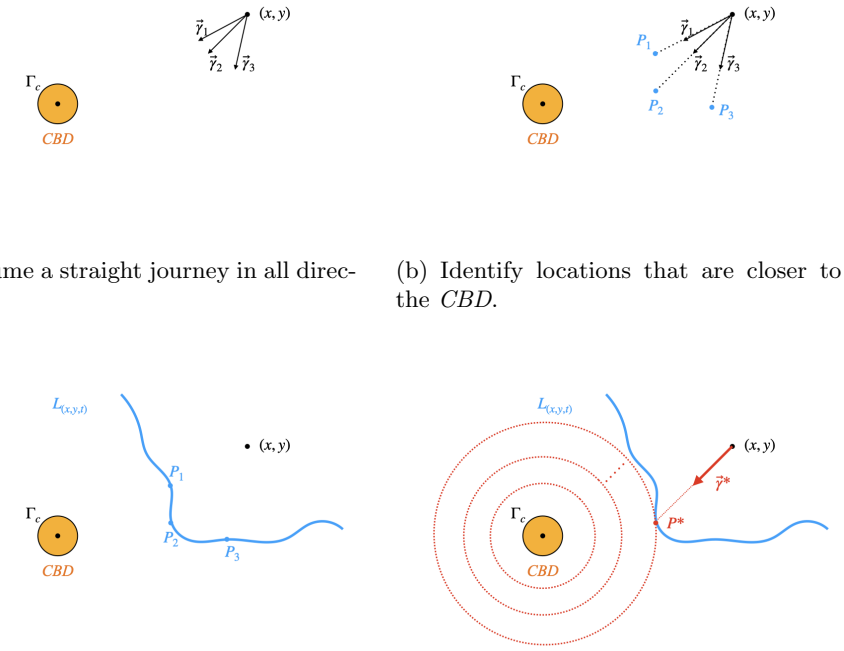

(a) Assume a straight journey in all directions.

(b) Identify locations that are closer to the *CBD*.

(c) Compare how far each location is from the *CBD*.

(d) Determine the optimal velocity direction.

Figure 3.2: **Graphical explanation of Strategy B.**

Figure 3.2 shows the entire local route-choice procedure for a traveler at fixed location (x, y) at time t. A traveler first considers different paths and calculates the straight-line distance of each path. Figure 3.2(a) shows three possible path directions; these are chosen arbitrarily, and there are infinitely many choices. For any fixed direction $\vec{\gamma} = (\gamma_1, \gamma_2)$ with $\|\vec{\gamma}\| = 1$, we denote the estimated travel distance from point (x, y) in this direction within period τ as $s_{\vec{\gamma}}(\tau)$. As the traveler can

obtain local traffic information, such as the travel speed U in the surrounding region, the travel distance can be obtained by solving the following ODE,

$$\begin{cases} \dfrac{ds_{\vec{\gamma}}(\tau)}{d\tau} = U\big(x + s_{\vec{\gamma}}(\tau)\gamma_1, y + s_{\vec{\gamma}}(\tau)\gamma_2, t\big), \\ s(0) = 0. \end{cases} \tag{3.8}$$

After a fixed time T_{perc} traveling straight in direction $\vec{\gamma}$, the traveler arrives at location $\big(x + s_{\vec{\gamma}}(T_{perc})\gamma_1, y + s_{\vec{\gamma}}(T_{perc})\gamma_2\big)$, denoted as point $P_{\vec{\gamma}}$. Figure 3.2(b) shows these possible locations, and we denote the set of points $P_{\vec{\gamma}}$ for all possible directions $\vec{\gamma}$ as

$$L_{(x,y,t)} := \{P_{\vec{\gamma}} = \big(x + s_{\vec{\gamma}}(T_{perc})\gamma_1, y + s_{\vec{\gamma}}(T_{perc})\gamma_2\big), \quad \forall \vec{\gamma} \text{ with } \|\vec{\gamma}\| = 1\}.$$

The set forms a closed curve, part of which is colored blue in Fig. 3.2(c).

Different directions $\vec{\gamma}$ may result in different travel distances, as these depend on the speed $U(x, y, t)$ along a path, which can vary. Thus, the route-choice strategy for a traveler at point (x, y) at time t involves determining the optimal traveling direction $\vec{\gamma}^*$, as shown in Fig. 3.2(d), such that the corresponding location $P^* := P_{\vec{\gamma}}$ is the closest point in the set $L_{(x,y,t)}$ to the *CBD* center (x_c, y_c). The velocity of that direction is given by

$$\frac{\mathbf{v}(x, y, t)}{||\mathbf{v}(x, y, t)||} = \underset{\vec{\gamma}=(\gamma_1,\gamma_2),\ ||\vec{\gamma}||=1}{\arg\min} \sqrt{(x + s_{\vec{\gamma}}(T_{perc})\gamma_1 - x_c)^2 + (y + s_{\vec{\gamma}}(T_{perc})\gamma_2 - y_c)^2}. \tag{3.9}$$

Point P^* satisfies the following property.

Theorem 3.2. *Suppose that curve $L_{(x,y,t)}$ is smooth. Center a circle $B(r)$ at the CBD center with a radius r. As the radius r increases from $r = 0$, the circle first reaches the set $L_{(x,y,t)}$ at one point P^* or at more points. In this case, the circle is tangential to the curve $L_{(x,y,t)}$ and the tangential point P^* is the optimal point we are seeking.*

Proof. Suppose that $B(r)$ is not tangential to $L_{(x,y,t)}$ at P^*. As P^* is the common point of the two curves, one of the two opposite tangential directions of $L_{(x,y,t)}$ must exist at P^* where the angle from the normal direction of the circle $B(r)$ at P^* is less than $\frac{\pi}{2}$. As shown in Fig. 3.3, because $L_{(x,y,t)}$ is smooth, there must exist a point $\tilde{P}$ in some domain of P^* on $L_{(x,y,t)}$ that is also within the circle $B(r)$, meaning that $\tilde{P}$ is closer to the *CBD* center than P^*. This contradicts the hypothesis. □

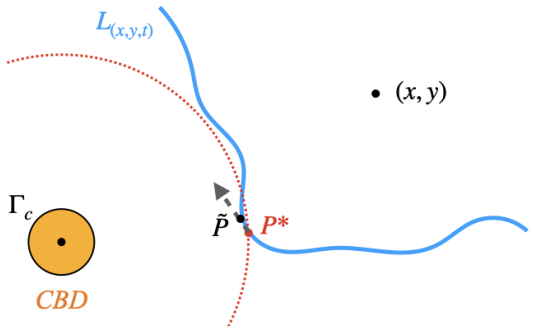

Figure 3.3: **Counterexample diagram as proof of Theorem 3.2.**

The complete model for route-choice Strategy B is constructed as follows:

$$\begin{cases} \rho_t(x,y,t) + \nabla \cdot \mathbf{F}(x,y,t) = q(x,y,t), \quad \forall (x,y) \in \Omega, \quad t \in [0,T], \\ \mathbf{F}(x,y,t) = \rho(x,y,t)\mathbf{v}(x,y,t), \quad \forall (x,y) \in \Omega, \quad t \in [0,T], \\ \dfrac{\mathbf{v}(x,y,t)}{U(x,y,t)} = \underset{\vec{\gamma}=(\gamma_1,\gamma_2),\ ||\vec{\gamma}||=1}{\arg\min} \sqrt{(x + s_{\vec{\gamma}}(T_{perc})\gamma_1 - x_c)^2 + (y + s_{\vec{\gamma}}(T_{perc})\gamma_2 - y_c)^2}, \\ U(x,y,t) = U_f(x,y)e^{-\beta(x,y)\rho^2(x,y,t)}, \quad \forall (x,y) \in \Omega, \quad t \in [0,T], \end{cases} \tag{3.10}$$

with the initial boundary conditions are

$$\begin{cases} \rho(x,y,0) = \rho_0(x,y), & \forall (x,y) \in \Omega, \\ \mathbf{F}(x,y,t) \cdot \mathbf{n}(x,y) = 0, & \forall (x,y) \in \Gamma_o \cup \Gamma_i, \quad t \in [0,T], \end{cases} \tag{3.11}$$

where the travel distance $s_{\vec{\gamma}}(\tau)$ can be obtained by solving the following ODE for each fixed location $(x,y) \in \Omega$ at any fixed time $t \in [0,T]$,

$$\begin{cases} \dfrac{ds_{\vec{\gamma}}(\tau)}{d\tau} = U\big(x + s_{\vec{\gamma}}(\tau)\gamma_1, y + s_{\vec{\gamma}}(\tau)\gamma_2, t\big), \\ s(0) = 0. \end{cases} \tag{3.12}$$

The initial boundary conditions are the same as those in Strategy A (Eq. (3.6)). The second equation in Eqs (3.12) is the boundary condition of $ds_{\vec{\gamma}}(\tau)$, which means that the travel distance is calculated from $\tau = 0$ at point (x,y) to $\tau = T_{perc}$ at some other point.

Remark 3.2. *In our work, we aim to develop mathematical models that simulate the behavior of conventional human drivers. These drivers possess only local perception of traffic dynamics and make route choices based on their judgment of local traffic conditions. In both strategies, drivers initially identify nearby temporary destinations instead of directly considering the distant final destination, as it is challenging for them to perform global and long-term path planning. Since they cannot access traffic information (such as density and speed) outside their local perception fields, the distance required to progress from the temporary destination to the final destination serves as the sole indicator for selecting a temporary destination. In Strategy A, travelers opt for equidistant temporary destinations. However, when moving from their current locations to temporary destinations within local perception regions, travelers prioritize travel time or cost over distance. They determine an optimal path, as in (3.1), to minimize travel costs to the temporary destinations. The travel cost is calculated using the eikonal equation in (3.2) and depends on the definition of the local travel cost per unit distance. In our numerical simulation, we set the local cost as the travel time per unit distance, but it may also depend on other factors. In Strategy B, travelers consistently strive to use the same travel time to reach a temporary destination closer to the final destination, thus reducing the total travel time when they eventually reach their final destination. In both strategies, travelers continually adjust their temporary destinations and travel directions en route to the final destination, always attempting to minimize travel costs based on the available local traffic information.*

Remark 3.3. *In Strategy A, travelers always choose moving directions to minimize the local travel cost to the temporary destinations. When vehicles are relatively distant from the final destination CBD, the temporary destinations are those places closer to the CBD. When vehicles are close to the CBD such that the CBD is already located within their local perception regions, the CBD serves*

both as the final destination and as the temporary destination. In this case, travelers simply find paths to minimize the travel cost to the CBD. For the travel cost ϕ^{loc} computed using the eikonal equation in (3.7), the boundary value is set as 0 at the destination. Also, the local cost $c > 0$. Thus, the negative gradient direction of ϕ^{loc} points towards the destination. For Strategy B, vehicles will continuously reduce the distance to the CBD. Their goal is to minimize the distance to the CBD as much as possible, so they will never drive away from the CBD.

4 Numerical Algorithms

In this section, we present numerical algorithms and a solution procedure for each model. To solve the problems numerically, we consider an unstructured triangular decomposition $\mathcal{T}_h$ of the computational domain Ω, where h is the maximum size of the triangular cells. We denote the total number of triangles in the spatial mesh as Nee and the n^{th} point in time as t_n. Section 4.1 presents the third-order RK method to solve the ODE problems in our model. In Section 4.2, we solve the eikonal equation via the second-order fast sweeping method, and in Section 4.3, we solve the conservation law via the high-order DG method with the PP and WENO limiters.

4.1 Runge-Kutta method

RK method [40] is the general method for solving ODE problems (e.g., Eq. 4.1).

$$\begin{cases} \dfrac{dw}{d\xi} = J(w(\xi)),\ \xi \in [a,b] \\ w(a) = 0. \end{cases} \tag{4.1}$$

We divide $[a,b]$ into discrete grid cells with size h_ξ and denote the n^{th} point as ξ_n. We denote the numerical solution of $w(\xi_n)$ as w^n. The numerical scheme is constructed as follows:

$$\begin{aligned} w^{(0)} &= w^n, \\ w^{(1)} &= w^{(0)} + h_\xi J(w^{(0)}), \\ w^{(2)} &= \frac{3}{4}w^{(0)} + \frac{1}{4}w^{(1)} + \frac{1}{4}h_\xi J(w^{(1)}), \\ w^{n+1} &= \frac{1}{3}w^{(0)} + \frac{2}{3}w^{(2)} + \frac{2}{3}h_\xi J(w^{(2)}). \end{aligned} \tag{4.2}$$

4.2 Second order fast sweeping method on triangular meshes

The eikonal equation is a particular static-state form of the Hamilton-Jacobi equation. The solution does not depend on time t. We take the following eikonal equation as an example.

$$\begin{cases} \|\nabla\phi(x,y,t)\| = c(x,y,t), & \forall (x,y) \in \Omega, \quad t \in [0,T], \\ \phi(x,y,t) = 0, & \forall (x,y) \in \Gamma_c, \quad t \in [0,T], \end{cases} \tag{4.3}$$

where the local travel cost c is given. In Eqs (3.7), we only need to change the computational domain and the boundary location.

The fast sweeping method begins with the following initialization. According to the boundary condition in Eqs (4.3), we assign the exact boundary values on Γ_c. Large values (e.g., 10^6) are assigned as the initial guess at all other grid points. For the second-order fast sweeping method, the solution from the first-order fast sweeping method is used as the initial guess at all other grid points. First, we need to choose multiple reference points $\mathbf{x}_{ref}^i,\ i = 1, 2, \ldots, R$, and sort all nodes according to their l_2-distances to the reference points in ascending and descending orders and record them as arrays S_i^+ and $S_i^-,\ i = 1, 2, \ldots, R$, respectively. We set $R = 4$ in this paper. Then, the following Gauss-Seidel iterations are performed after initialization: For all of $i = 1, 2, \ldots, R,\ j = +, -$, for each vertex $C \in S_i^j$ and every triangular mesh associated with C, the local solver is applied. Here, a triangular mesh (Fig. 4.1) with three nodes is taken as an example.

$A = (x_A, y_A),\ B = (x_B, y_B)$, and $C = (x_C, y_C)$. Under the assumption that ϕ_A and ϕ_B are given, and we need to modify ϕ_C, we denote $\alpha = \angle B, \beta = \angle A, \gamma = \angle C$.

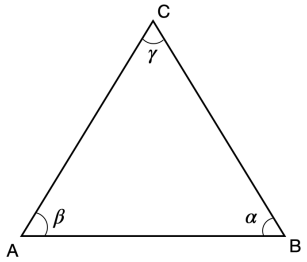

Figure 4.1: **A triangular cell.**

1. If the following two conditions are satisfied

   (1) $|T_B - T_A| \le |AB|c(C)$, where $|AB|$ represents the length of $\bar{AB}$ and $c(C)$ is the value of $c(x, y, t)$ at point C at time t;

   (2) $\theta := arcsin(\dfrac{|T_B - T_A|}{|AB|c(C)})$, $max(0, \alpha - \frac{\pi}{2}) \le \theta \le \frac{\pi}{2} - \beta$ or $\alpha - \frac{\pi}{2} \le \theta \le min(0, \frac{\pi}{2} - \beta)$, then for a first-order fast sweeping method, we compute

$$\phi_C^{new} = min\{\phi_C^{old}, \frac{1}{2}(\phi_A + \phi_B + \frac{sin(\beta - \alpha)}{sin\gamma}(\phi_A - \phi_B) + \frac{2sin\alpha sin\beta}{sin\gamma}\sqrt{|AB|^2c^2(C) - (\phi_A - \phi_B)^2})\}. \tag{4.4}$$

   For a second-order fast sweeping method, we first denote that

$$D_A = \begin{pmatrix} x_A - x_B & y_A - y_B \\ x_A - x_C & y_A - y_C \end{pmatrix}, \quad D_B = \begin{pmatrix} x_B - x_A & y_B - y_A \\ x_B - x_C & y_B - y_C \end{pmatrix}, \quad D_C = \begin{pmatrix} x_C - x_A & y_C - y_A \\ x_C - x_B & y_C - y_B. \end{pmatrix} \tag{4.5}$$

   Then, we get

$$\nabla\phi_A = D_A^{-1}\begin{pmatrix} \phi_A - \phi_B \\ \phi_A - \phi_C^{old} \end{pmatrix}, \quad \nabla\phi_B = D_B^{-1}\begin{pmatrix} \phi_B - \phi_A \\ \phi_B - \phi_C^{old} \end{pmatrix}. \tag{4.6}$$

   We use $\phi_A, \phi_B, \nabla\phi_A$, and $\nabla\phi_B$ to update ϕ_C:

$$\phi_C^{new} = min\{\phi_C^{old}, \frac{1}{4}(2\phi_A + 2\phi_B + \tilde{m} + \tilde{n} + \frac{sin(\beta - \alpha)}{sin\gamma}\tilde{M} + \frac{2sin\alpha sin\beta}{sin\gamma}\sqrt{|AB|^2c^2(C) - \tilde{M}^2})\}, \tag{4.7}$$

where

$$\begin{aligned}\tilde{M} &= 2\phi_A - \phi_B + \tilde{m} - \tilde{n},\\ \tilde{m} &= (x_C - x_A, y_C - y_A)^T \cdot \nabla\phi_A,\\ \tilde{n} &= (x_C - x_B, y_C - y_B)^T \cdot \nabla\phi_B.\end{aligned} \tag{4.8}$$

2. If any of the above conditions is not satisfied, then

$$\phi_C = min\{\phi_C, \phi_A + |AC|c(C), \phi_B + |BC|c(C)\}. \tag{4.9}$$

Convergence is declared if

$$\|\phi^{new} - \phi^{old}\| \le \delta, \tag{4.10}$$

where δ is a given convergence threshold value. $\delta = 10^{-14}$ and the L^∞ norm are used in our computation for the first-order fast sweeping method, and $\delta = 10^{-3}$ and the L^∞ norm are used for the second-order fast sweeping method. Finally, we can modify $\nabla\phi_C$ with ϕ_C^{new}:

$$\nabla\phi_C^{new} \approx D_C^{-1}\begin{pmatrix}\phi_C^{new} - \phi_A\\ \phi_C^{new} - \phi_B\end{pmatrix}. \tag{4.11}$$

4.3 DG method with a PP limiter and a WENO limiter

The conservation law and its initial condition are as follows:

$$\begin{cases}\rho_t + f(\rho)_x + g(\rho)_y = s, & \forall (x,y)\in\Omega, t\in[0,T],\\ \rho(x,y,0) = \rho_0(x,y), & \forall (x,y)\in\Omega.\end{cases} \tag{4.12}$$

We use high-order RK DG methods to solve the above nonlinear hyperbolic conservation law. In combination with the Lax–Friedrichs (LF) numerical flux [25], we use the high-order RK method for temporal discretization [40] and the DG method for spatial discretization. We add a high-order WENO limiter [60, 57] to the DG method to avoid numerical oscillations. Moreover, a high-order PP limiter [55] is added to theoretically avoid a nonphysical negative value of the density.

In DG methods, the solutions consist of piecewise discontinuous functions. We denote the finite element solution space as

$$V_h^k = \left\{p : p|_K \in P^k(K), \forall K \in \mathcal{T}_h\right\},$$

where $P^k(K)$ denotes the set of polynomials of degree up to k in cell K. We aim to find $\rho_h(x,y,t) \in V_h^k$, such that for any test functions $v_h \in V_h^k$ and any cell $K \in \mathcal{T}_h$, we have

$$\int_K (\rho_h)_t v_h dxdy - \int_K \big(f(\rho_h)(v_h)_x + g(\rho_h)(v_h)_y\big)dxdy + \int_{\partial K}\hat{F}^n v_h ds = \int_K s v_h dxdy. \tag{4.13}$$

In this scheme, $\hat{F}^n$ is the numerical flux defined on cell boundaries and is an approximation to $\mathbf{F}\cdot\mathbf{n}$, where $\mathbf{F} = (f,g)^T$ and $\mathbf{n}$ denotes the unit outward normal vector of the boundary ∂K. In our numerical examples, we adopt the following LF numerical flux

$$\hat{F}^n(\rho_h^{int}, \rho_h^{ext}, \mathbf{n}) = \frac{1}{2}(\mathbf{F}(\rho_h^{int})\cdot\mathbf{n} + \mathbf{F}(\rho_h^{ext})\cdot\mathbf{n} - \alpha(\rho_h^{ext} - \rho_h^{int})),$$

where $\alpha = \max_\rho \left|\mathbf{F}'(\rho)\cdot\mathbf{n}\right|$. The superscripts ext and int represent the values of ρ_h read from the exterior and interior of K respectively. After we apply the DG method in space, the semi-discrete scheme (4.13) can be written as a set of ODE problems. We apply the third-order RK time-marching method in Section 4.1.

For traffic flow problems, the density ρ must be physically nonnegative; therefore, we apply a PP limiter to modify the numerical solution $\rho_h(x, y, t)$. For convenience, we omit the independent variables x, y, t in the following schemes. In each cell K, we let $\rho_h^n|_K = \rho_K^n$ and denote the cell average as

$$\bar{\rho}_K^n = \frac{1}{|K|} \int_K \rho_K^n dxdy.$$

Assuming $\bar{\rho}_K^n \geq m$, we replace the polynomial ρ_K^n with the following modified polynomial $\tilde{\rho}_K^n$ using a linear scaling limiter:

$$\tilde{\rho}_K^n = \theta \left(\rho_K^n - \bar{\rho}_K^n\right) + \bar{\rho}_K^n, \quad \theta = \min\left\{\left|\frac{m-\bar{\rho}_K^n}{m_K^n - \bar{\rho}_K^n}\right|, 1\right\}, \tag{4.14}$$

where $m_K^n = \min_K \rho_K^n$. In [55], it is proved that this limiter preserves the lower bound m of the solution and does not affect the original high-order accuracy of DG methods. Moreover, after the application of the PP limiter at time level n, the cell average $\bar{\rho}_K^{n+1}$ at the next time level will be automatically nonnegative.

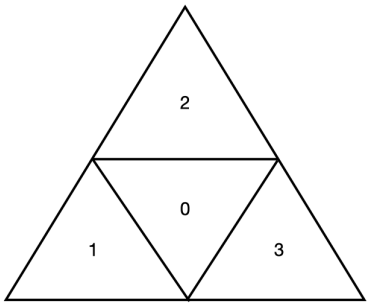

Figure 4.2: **The compact stencil in the WENO limiter.**

In addition to the PP limiter, we add a high-order WENO limiter to the DG method to avoid numerical oscillations. First, we need to identify the troubled cells via the KXRCF technique [23]. Then, we replace the DG polynomial in each troubled cell with a new smooth polynomial. For simplicity, we omit t and the related superscript n. We relabel the troubled cell and its three neighboring cells as shown in Fig. 4.2. We denote this stencil as $S = \{K_0, K_1, K_2, K_3\}$. The DG solution polynomials ρ_h on cells $K_i,\ i = 0,\ 1,\ 2,\ 3$ are first denoted as $q_i(x, y),\ i = 0,\ 1,\ 2,\ 3$, respectively. Then, the following modifications are made:

$$\tilde{q}_i(x, y) = q_i(x, y) - \overline{\overline{q}}_i + \overline{\overline{q}}_0,\ i = 0,\ 1,\ 2,\ 3, \tag{4.15}$$

where

$$\overline{\overline{q}}_i = \frac{1}{|K_0|} \int_{K_0} q_i(x, y)\mathrm{d}x\mathrm{d}y,\ i = 0,\ 1,\ 2,\ 3. \tag{4.16}$$

The nonlinear WENO reconstruction polynomial $\tilde{\rho}_{K_0}$ is defined by a convex combination of these modified polynomials:

$$\tilde{\rho}_{K_0}(x, y) = \omega_0 q_0(x, y) + \sum_{i=1}^{3} \omega_i \tilde{q}_i(x, y), \tag{4.17}$$

with

$$\sum_{i=0}^{3} \omega_i = 1. \tag{4.18}$$

To obtain $\omega_i,\ i=0,\ 1,\ 2,\ 3$, we need to compute the smoothness indicators $\beta_i,\ i=0,\ 1,\ 2,\ 3$:

$$\beta_i = \sum_{|\ell|=1}^{k} |K_0|^{|\ell|-1} \int_{K_0} \left(\frac{\partial^{|\ell|}}{\partial x^{\ell_1} \partial y^{\ell_2}} q_i(x,y) \right)^2 \mathrm{d}x\mathrm{d}y, \tag{4.19}$$

where $l=(l_1,l_2)$. Then we can get

$$\omega_i = \frac{\bar{\omega}_i}{\sum_{j=0}^{3} \bar{\omega}_j}, \quad \bar{\omega}_j = \frac{\gamma_j}{(\varepsilon+\beta_j)^2}, \quad i,j=0,\ 1,\ 2,\ 3. \tag{4.20}$$

4.4 Solution procedures

In our problem, we assume that all travelers ultimately reach the *CBD*, at which time there is no further traffic demand in the city. Hence, we set an indicator t_{end} that represents the time at which all vehicles reach the *CBD*. For this purpose, we let $f_{CBD}(t)$ (in veh) be the cumulative number of vehicles that reach the *CBD* by time t, as follows:

$$f_{CBD}(t) = \int_0^t \oint_{\Gamma_c} (\mathbf{F}\cdot\mathbf{n})(x,y,\tau) ds d\tau, \quad t\in[0,T], \tag{4.21}$$

where $\mathbf{n}(x,y)$ is the unit normal vector on the boundary Γ_c. We let $D(t)$ (in veh) be the cumulative traffic demand at time t, as follows:

$$D(t) = \int_0^t \iint_{\Omega} q(x,y,\tau) dx dy d\tau, \quad t\in[0,T]. \tag{4.22}$$

We then define t_{end} as the time at which the following condition is satisfied:

$$\frac{|D(t_{end}) - f_{CBD}(t_{end})|}{D(t_{end})} < 10^{-5}. \tag{4.23}$$

We then stop the computation.

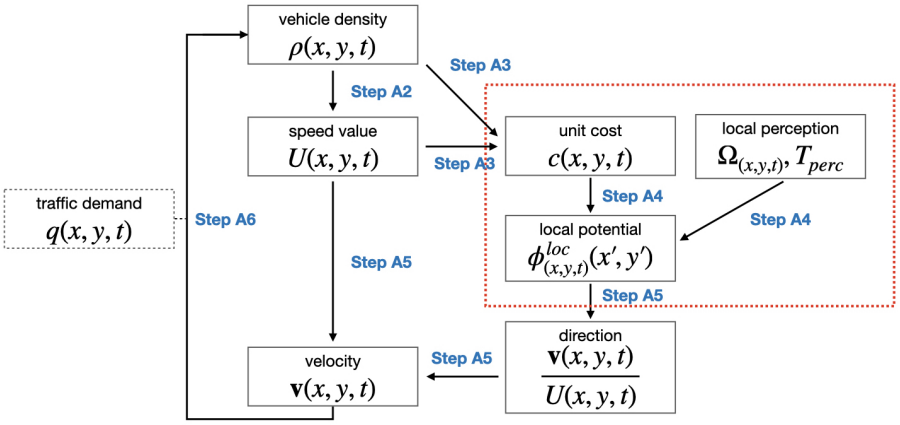

Figure 4.3: **Solution procedure for Strategy A.**

In Strategy A, starting from density ρ^n at time t_n (for simplicity, we omit the subscript K), we obtain the density ρ^{n+1} in the following steps. Figure 4.3 illustrates the procedure, where the red

dotted box highlights the route-choice strategy.

Solution procedure for Strategy A

Step A1 At $t = t_n$, suppose that the density ρ^n is already known, and the density at the initial time is given by the initial condition, as follows: $\rho(x, y, 0) = \rho_0(x, y)$.

Step A2 Compute the speed value U using Eq. (2.1).

Step A3 Compute the local cost c using Eq. (2.4).

Step A4 Use the second-order fast sweeping method to solve Eqs (3.7) in $\Omega_{(x,y,t)}$ to obtain the temporary total travel cost $\phi^{loc}_{(x,y,t)}$ at each mesh grid.

Step A5 Set the direction using the route-choice strategy Eq. (3.3). Combine this with the speed obtained in Step A2 to solve the speed vector $\mathbf{v}$.

Step A6 Use the RK method and third-order DG scheme with PP limiter and WENO limiter to solve the time-dependent conservation law (Eq. (2.3)) to obtain the density ρ^{n+1} at $t = t_{n+1}$ by Eq. (4.13) and Eq. (4.2).

Step A7 Stop the iteration process when $t \geq t_{end}$.

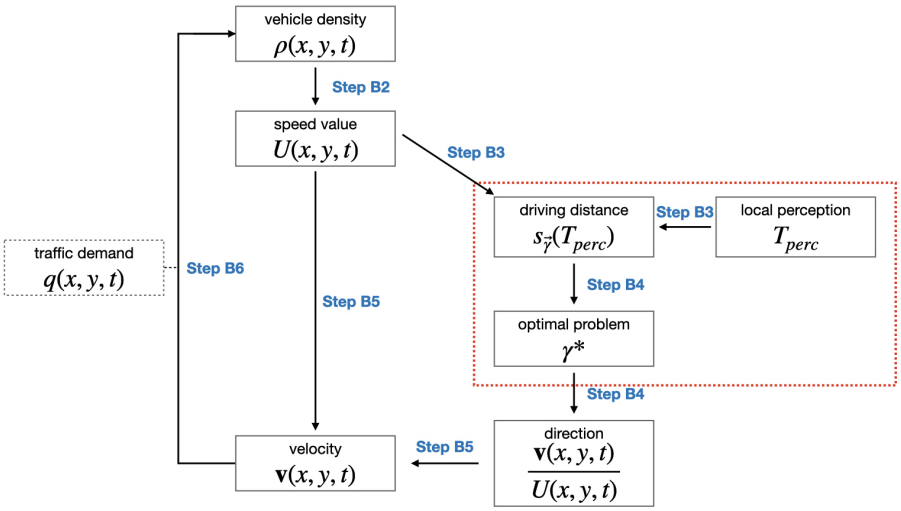

Figure 4.4: **Solution procedure for Strategy B.**

Similarly, for Strategy B, starting from the density ρ^n at time t_n, we obtain the density ρ^{n+1} by performing the following steps in a Euler forward time discretization process (see Fig. 4.4).

Solution procedure for Strategy B

Step B1 At $t = t_n$, suppose that density ρ^n is already known.

Step B2 Compute the speed value U using Eq. (2.1).

Step B3 Use the Euler method to solve the ODE (Eq. (3.8)) to obtain the travel distance $s_{\vec{\gamma}}$ in each direction.

Step B4 Compute the optimization problem (Eq. (3.9)) and set the direction.

Step B5 Combine the direction with the speed obtained in Step B2 to solve the speed vector $\mathbf{v}$.

Step B6 Apply the RK method and third-order DG scheme with the PP limiter and the WENO limiter to solve the time-dependent conservation law (Eq. (2.3)) to obtain the density ρ^{n+1} at $t = t_{n+1}$ using Eq. (4.13) and Eq. (4.2).

Step B7 Stop the iteration process when $t \geq t_{end}$.

5 Numerical Examples

In this section, numerical examples are given to demonstrate the effectiveness of our model and the convergence of the solution algorithm. We also compare various route-choice strategies.

5.1 Example 1: An urban city with a circular *CBD*

5.1.1 Problem Settings

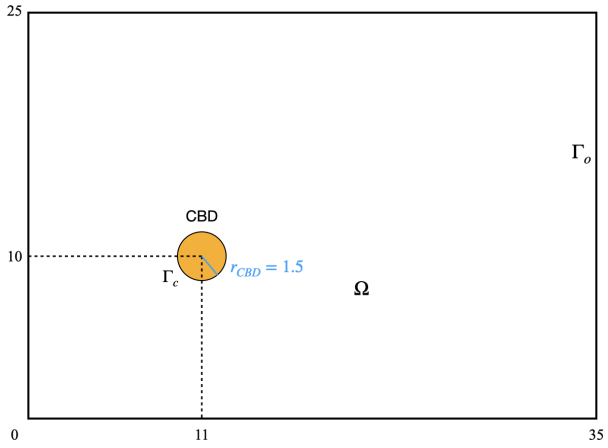

Figure 5.1: **The modeled region in the numerical example.**

As shown in Fig. 5.1, the city is a $[0\ km, 35\ km] \times [0\ km, 25\ km]$ rectangular region containing a circular *CBD* with radius $r_{CBD} = 1.5\ km$. The *CBD* center is located at $(x_c, y_c) = (11\ km, 10\ km)$. In the speed function given by Eq. (2.1), we use the following parameter settings:

$$\rho_j = 6000[1 - 0.01\ dist(x, y)]$$

and $C = 8\ km/h$. The free-flow speed is defined as

$$U_f(x, y) = U_{\max}\left[1 + \gamma_2 dist(x, y)\right],$$

where $U_{\max} = 30\ km/h$ and $\gamma_2 = 4 \times 10^{-3}\ \mathrm{km}^{-1}$ are parameters, and

$$dist\,(x, y) = \sqrt{(x - 11)^2 + (y - 10)^2}$$

is the distance from location (x, y) to the *CBD* center. The factor $[1 + \gamma_2 dist(x, y)]$ is used to express the greater free-flow speed in the domain further from the *CBD*, where there are fewer junctions. The traffic demand is set as

$$q(x, y, t) = q_{\max} [1 - \gamma_1 dist(x, y)] g(t),$$

where $q_{\max} = 400\ veh/km^2/h$ is the maximum traffic demand and $\gamma_1 = 0.01\ km^{-1}$ is a parameter. The factor $[1 - \gamma_1 dist(x, y)]$ indicates that there is a higher traffic demand in the area closer to the *CBD*, and $g(t)$ is a non-negative and time-varying function defined by

$$g(t) = \begin{cases} t, & t \in [0h, 1h], \\ 1, & t \in (1h, 2h], \\ -\frac{4}{5}(t-3) + \frac{1}{5}, & t \in (2h, 3h], \\ \frac{1}{5}, & t \in (3h, 5h], \\ 0, & otherwise. \end{cases} \tag{5.1}$$

In Strategy A, we use $c(x, y, t) = \dfrac{\kappa}{U(x, y, t)}$, which means that the local potential function $\phi^{loc}_{(x,y,t)}(x', y')$ defined in the local region $\Omega_{(x,y,t)}$ is simply the travel time value. We set $\kappa = 90\ \$/h$. For simplicity, when defining the feasible region $\tilde{\Omega}_{(x,y)} := B((x, y), r_0(x, y, t))$, we set $r_0(x, y, t)$ as a constant, i.e., $r_0(x, y, t) \equiv 0.25\ km$. In strategies A and B, we set $T_{perc} = 30\ s$ to represent the perception of travelers.

For comparison, we also test three cases of the original global route-choice strategies described in Section 2.3, denoted as strategies C, D, and E. For Strategy C, we set the local cost function to

$$c(x, y, t) \equiv 1, \quad \forall (x, y) \in \Omega, \quad t \in [0, T], \tag{5.2}$$

which is independent of the density. The global cost function ϕ is thus the travel distance to the *CBD*. To minimize the travel distance, the path choice strategy requires traveling directly to the *CBD*. Hence, in this special case, travelers do not consider any information about the density of the city. In Strategy D, we set the local cost function to

$$c(x, y, t) = \frac{\kappa}{U(x, y, t)}, \quad \forall (x, y) \in \Omega, \quad t \in [0, T], \tag{5.3}$$

where κ is the value of time and $\dfrac{\kappa}{U}$ represents the local travel-time cost. Hence, the route-choice strategy is to minimize the global travel time ϕ to the *CBD*. In Strategy E, the total travel cost ϕ is computed using Eq. (2.6). The various strategies tested in these numerical examples are listed in Table 5.1.

Strategy	**Perception**	**Destination**	**Principle**	**Section**
A	Local	Temporary	Minimize the travel time	3.1
B	Local	*CBD*	Move closer to the *CBD* in a short time	3.2
C	None	*CBD*	Minimize the travel distance	2.3
D	Global	*CBD*	Minimize the instantaneous travel time	2.3
E	Global	*CBD*	Minimize the actual travel time	2.3

Table 5.1: **Various route-choice strategies.**

The numerical initial boundary conditions are set as follows.

1. On the solid wall boundary $\Gamma_o \cup \Gamma_i$, we set the normal numerical flux $\hat{F}^n$ to 0.

2. On the *CBD* boundary Γ_c, we set $\phi = 0$ in strategies C and D, as Γ_c is the destination. We assume that the capacity of the *CBD* is sufficiently large such that no travelers leave the *CBD* after they have arrived at the *CBD*. Moreover, vehicles can enter the *CBD* without congestion, and therefore the speed is the free-flow speed inside the *CBD*.
3. On the local destination boundary $\Gamma_{(x,y,t)}$ in Strategy A, we set $\phi^{loc}_{(x,y,t)} = 0$.
4. We set the initial time as $t = 0\ h$. The initial condition of the conservation law is $\rho = \rho_0 = 0\ veh/km^2$ in Ω.

5.1.2 Numerical Results

To solve the conservation law, we adopt the third order DG methods. For the computational domain decomposition, we use an unstructured mesh with Nee triangles. We use a fine mesh near the *CBD* and in areas with predictable traffic complexity, as well as for further needs (such as setting the blockage area in Section 5.2). We use a coarse mesh elsewhere to save on total computational costs. Figure 5.2 shows the mesh with $Nee = 12,116$ triangles.

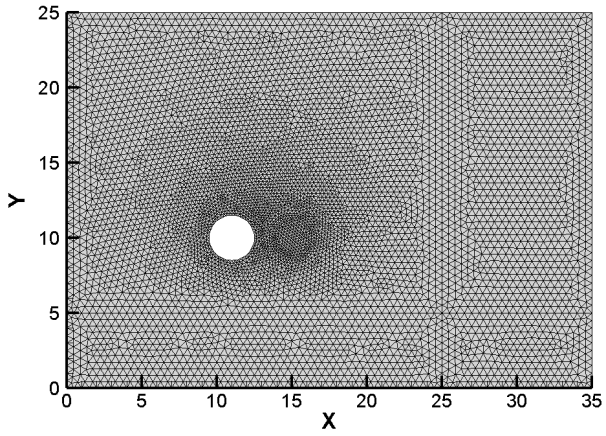

Figure 5.2: **Triangular mesh with** $Nee = 12116$**.**

We first test the convergence of the numerical algorithm by refining the mesh. The results for the various route-choice strategies are similar, and thus for brevity we only show the results of Strategy D. We take the time $t = 2\ h$. The one-dimensional cuts of the density along $x = 25\ km$ and $y = 5\ km$ are shown in Fig. 5.3 under different meshes. A good convergence exists among the meshes, and the results are sufficiently accurate, with $Nee = 12,116$ triangles. Hence, we adopt $Nee = 12,116$ (as shown in Fig. 5.2) for further analysis.

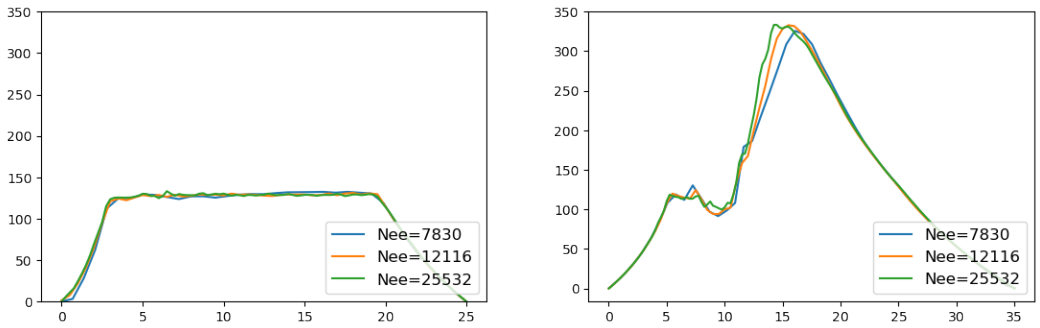

(a) $x = 25$ (b) $y = 5$

Figure 5.3: **Convergence curves of the density at $t = 2h$.**

Table 5.2 shows the CPU time required to solve the entire model (from initial time to final time t_{end}) with each strategy. The models using local route-choice strategies A or B require more time to solve than the global models using strategies C, D, or E. Strategy B requires the most time because we use the enumeration method (i.e., 400 possible directions of travel) to solve the optimization problem at each time step and each grid point. Since the RK method will greatly increase the calculation time, we apply Euler method to solve the ODE in Strategy B. Moreover, for each enumeration, we solve the ODE with the Euler method, which requires 10 steps each time. However, for the local eikonal equations and ODE evaluations at each grid point, the computations are independent at each time point. As the third-order DG scheme for the conservation law needs only a local small computational stencil, parallel computing can be used to swiftly perform the computations for local route-choice strategies. We can also divide the city into several regions and solve the model for each region independently. Thus, only a small amount of information must be transferred between the models for the various regions.

Strategy	CPU time (s)	t_{end} (h)	CPU time/t_{end} (s/h)
A	335,329	6.0197	55,705.27
B	1,798,319	6.2810	286,310.94
C	21,963	6.7421	3,257.59
D	254,452	5.8715	43,336.80
E	152,104	5.4829	27,741.52

Table 5.2: **CPU time required to solve the entire model using various different strategies.**

In the local route-choice strategies, T_{perc} is an interesting parameter whose value may vary with the scenario. Hence, we conduct a sensitivity analysis of this parameter. Recall that t_{end} is the time by which all travelers have reached the *CBD*, as defined in Section 4.4. We consider t_{end} to be an indicator of traffic efficiency, and we denote another indicator, t_{avg}, as the average travel time of all vehicles, as follows:

$$t_{avg} = \frac{\int_0^{t_{end}} \iint_\Omega \rho(x, y, t) dx dy dt}{D(t_{end})}. \tag{5.4}$$

The values of these two indicators correspond to various strategies, and those of T_{perc} are shown in Table 5.3. We can see that t_{avg} is positively related to t_{end}. Generally, travelers following strategies A and B travel faster than those following Strategy C and slower than those following strategies D and E, and Strategy E performs better than Strategy D. This is consistent with a priori estimates,

as Strategy D considers global instantaneous traffic information and Strategy E is able to predict global real traffic information, whereas strategies A and B only consider local traffic information and Strategy C does not consider any traffic information. In strategies A and B, as T_{perc} increases the local perception of traffic conditions improves and the local route-choice region expands. Table 5.3 also shows that the values of t_{end} and t_{avg} decrease as T_{perc} increases; moreover, Strategy A is more sensitive to T_{perc} than Strategy B, and Strategy A performs better with a large T_{perc}. If T_{perc} and r_0 are sufficiently large, the performance of Strategy A is almost the same as that of Strategy D. In the following sections, we set $T_{perc} = 30\ s$ for further analysis.

Strategy	T_{perc}/s	t_{end}/h	t_{avg}/h
A	30	6.0184	0.6437
A	15	6.0054	0.6927
A	5	6.0169	0.7815
A	2	6.0473	0.8089
B	30	6.2810	0.8389
B	15	6.4929	0.8764
B	5	6.6026	0.8983
B	2	6.6271	0.9057
C	\	6.7421	0.9192
D	\	5.8715	0.4773
E	\	5.4829	0.4064

Table 5.3: **Overall performances of various strategies and T_{perc}.**

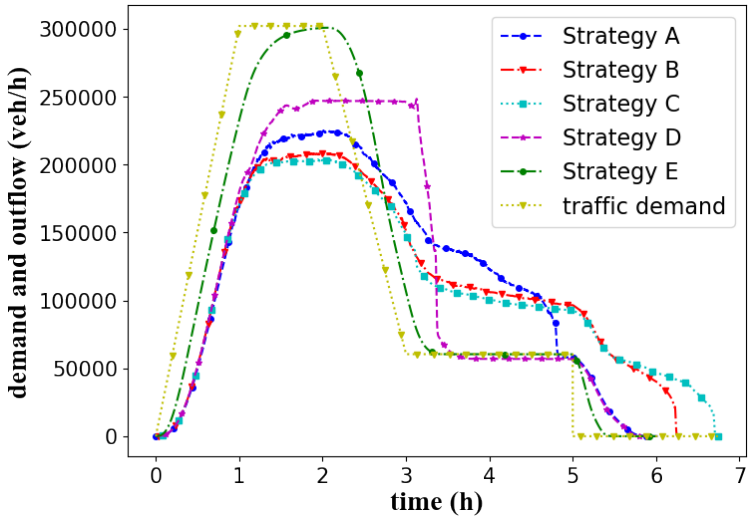

Figure 5.4: **Traffic demand and outflow.**

In the above analysis, the overall performances of the different strategies are compared in terms of the indicators t_{end} and t_{avg}. We now compare their performance over time. Consider the city's total hourly traffic demand at time t (in veh/h), defined as follows:

$$\tilde{D}(t) := \frac{d}{dt}D(t) = \iint_{\Omega} q(x, y, t)dxdy, \quad t \in [0, T], \tag{5.5}$$

and the total outflow rate through the *CBD* boundary at time t (in veh/h), defined as follows:

$$\tilde{f}_{CBD}(t) := \frac{d}{dt} f_{CBD}(t) = \oint_{\Gamma_c} (\mathbf{F} \cdot \mathbf{n})(x, y, t) ds, \quad t \in [0, T]. \tag{5.6}$$

Figure 5.4 shows a comparison of $\tilde{D}(t)$ and $\tilde{f}_{CBD}(t)$ for the various strategies. The numerical results show that the areas under the curves are all the same, confirming that all travelers have reached the *CBD* by the end of the modeled period. As shown by the yellow line, the traffic demand grows quickly in $[0\ h, 1\ h]$ and then maintains the maximum value for $[1\ h, 2\ h]$. After a short delay, the outflows through the *CBD* boundary increase for all strategies. As travelers have a global perception of traffic information, the outflows in strategies D and E (the purple line and green line, respectively, in Fig. 5.4) increase rapidly and then the outflow of Strategy D remains a high level and that of Strategy E keeps growing rapidly, which shows the efficiency and effectiveness of the global route-choice strategy. In contrast, in strategies A and B (the navy-blue line and red line, respectively), the maximum outflow intensity is relatively small because only local traffic information is available to each traveler. In Strategy C, in which travelers do not consider any traffic information and travel directly to the *CBD*, the outflow (the light-blue line) is always lagging, and the maximum outflow intensity can only be maintained at a low level.

When the traffic demand starts to decrease from $t = 2\ h$, the outflow curves for strategies D and E decrease rapidly. This also occurs for the other strategies but their respective decreases are slower. The total demand remains at a positive constant value for a period and then decreases to 0 veh/h. The outflows in strategies D and E rapidly decrease to the same constant, as most travelers have already reached the *CBD* by this time. The outflow curves for the other strategies remain at a relatively high level and their rates of descent are slower because the large amount of traffic demand generated has not yet reached the *CBD*.

After $t = 5\ h$, the traffic demand falls to 0 veh/h, and the outflow intensity for all strategies decreases to 0 veh/h thereafter. This takes a long time to occur for Strategy C, as no traffic information is considered.

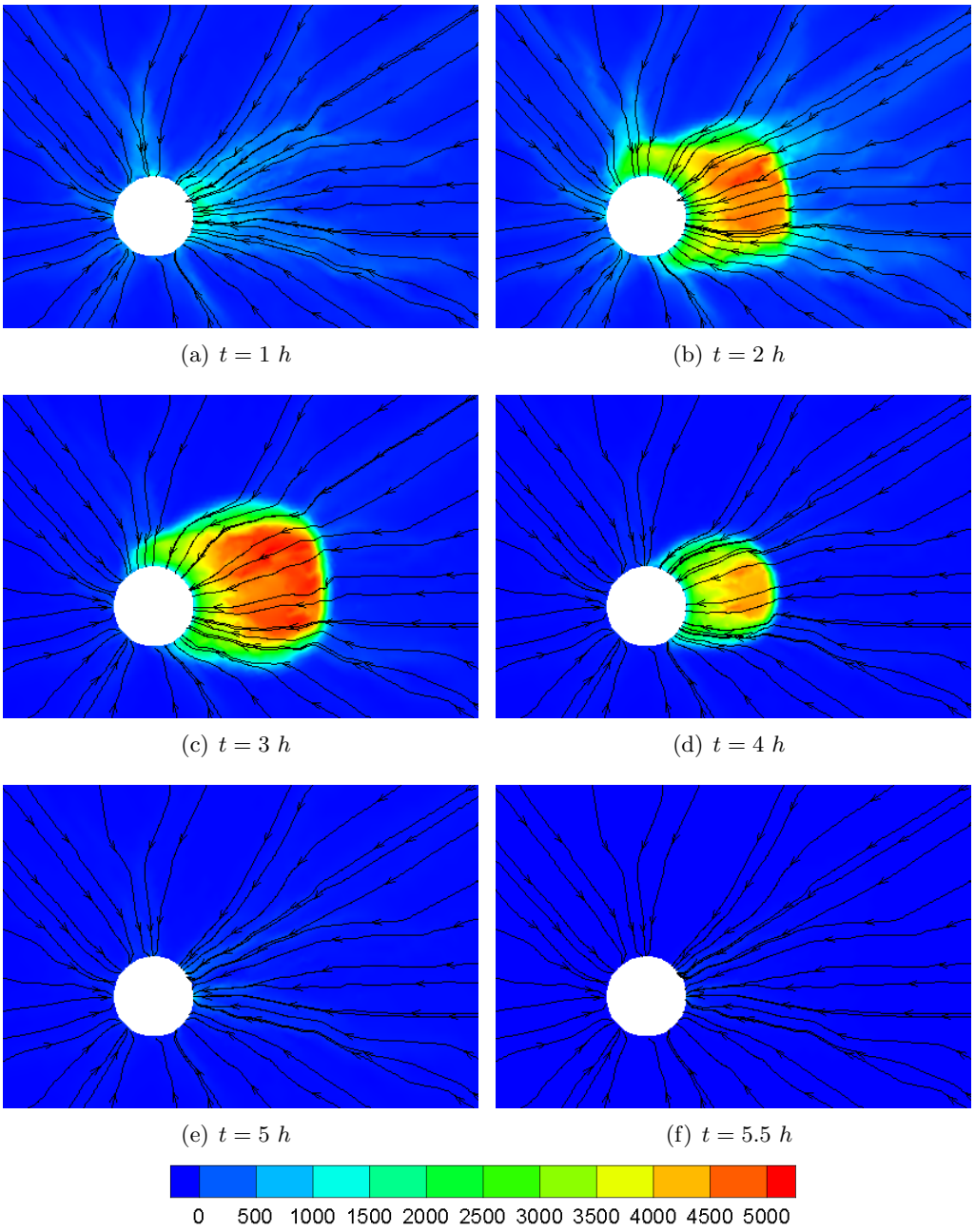

Figure 5.5: **Density and velocity plots for Strategy A.**

We next compare the spatial distribution of the density and the velocity vector for various strategies and times. Figure 5.5 shows the density and velocity plots for Strategy A. To clearly visualize the details, we only show zoom-in figures of the region near the *CBD* of all plots. In Fig. 5.5(a), the density is initially low. As increasing numbers of vehicles travel toward the *CBD*, the main high-density area is concentrated to the northeast of the *CBD* (Fig. 5.5(b)-(c)). Travelers are able to choose a curved path to avoid the high-density area and thus their driving directions change significantly, particularly near the contours with large density changes. Far away from the *CBD*, the density of vehicles is low and thus vehicles travel in near-straight lines. However, these straight lines do not point toward the *CBD* center; they are more likely to pass tangentially along the boundaries of the high-density area. As demand decreases to 0 veh/h, as shown in Fig. 5.5(d)-

(f), the main area of the city returns to a non-congested state and more vehicles move along a less curved path to the *CBD*. All of the vehicles reach the *CBD* by $t_{end} = 6.0184h$.

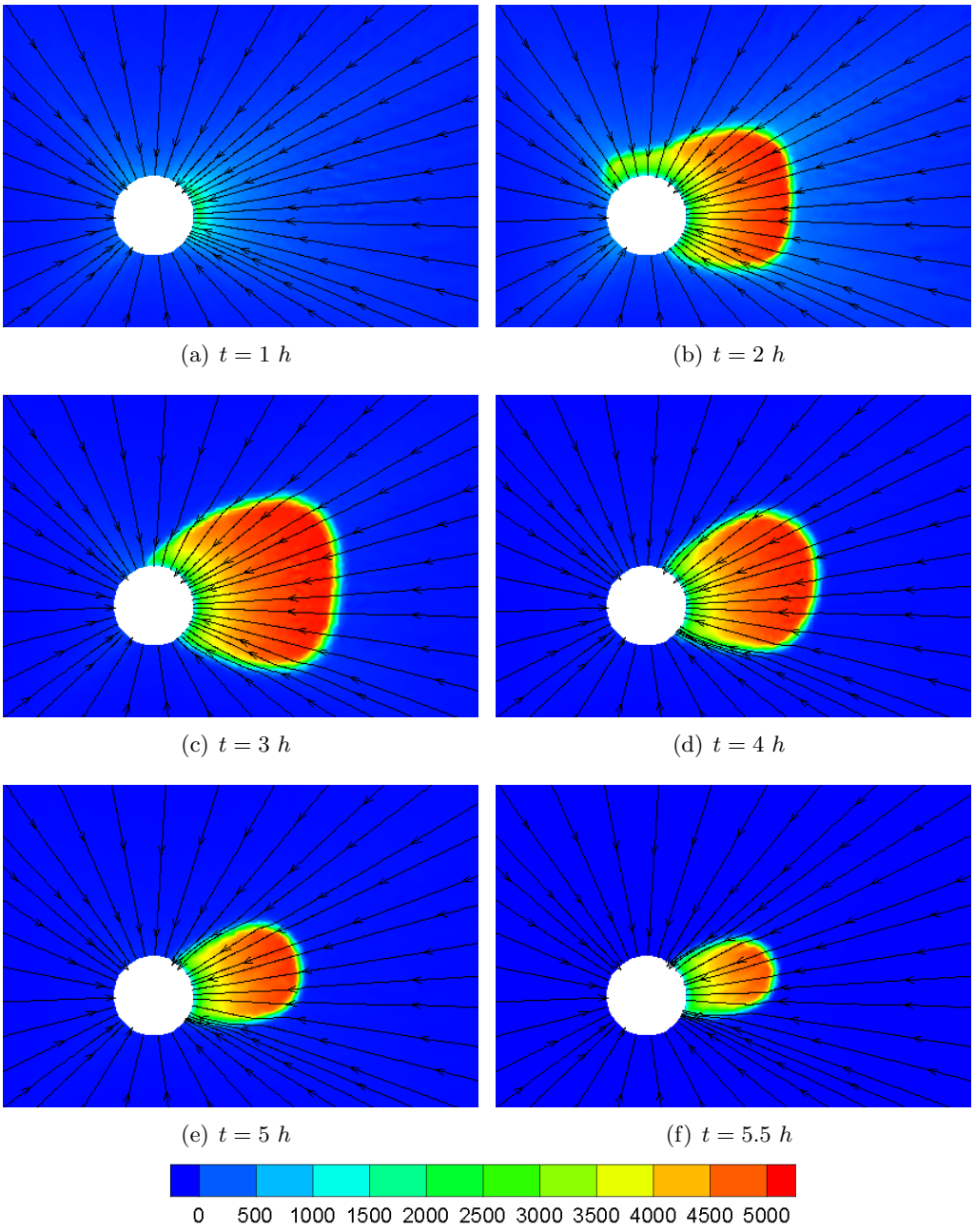

Figure 5.6: **Density and velocity plots for Strategy B.**

Figure 5.6 shows the density and velocity plots for Strategy B. As in Strategy A, there is no congestion in the region far away from the *CBD*. As the traffic demand increases, the high-density area to the east of the *CBD* increases in size. The traffic then gradually dwindles until all vehicles have reached the *CBD* (Fig. 5.6(e)-(f)) and there is no new traffic demand. Travelers are also able to choose curved paths to avoid the high-density area, especially near contours with large density changes. All of the vehicles reach the *CBD* by $t_{end} = 6.2810\ h$.

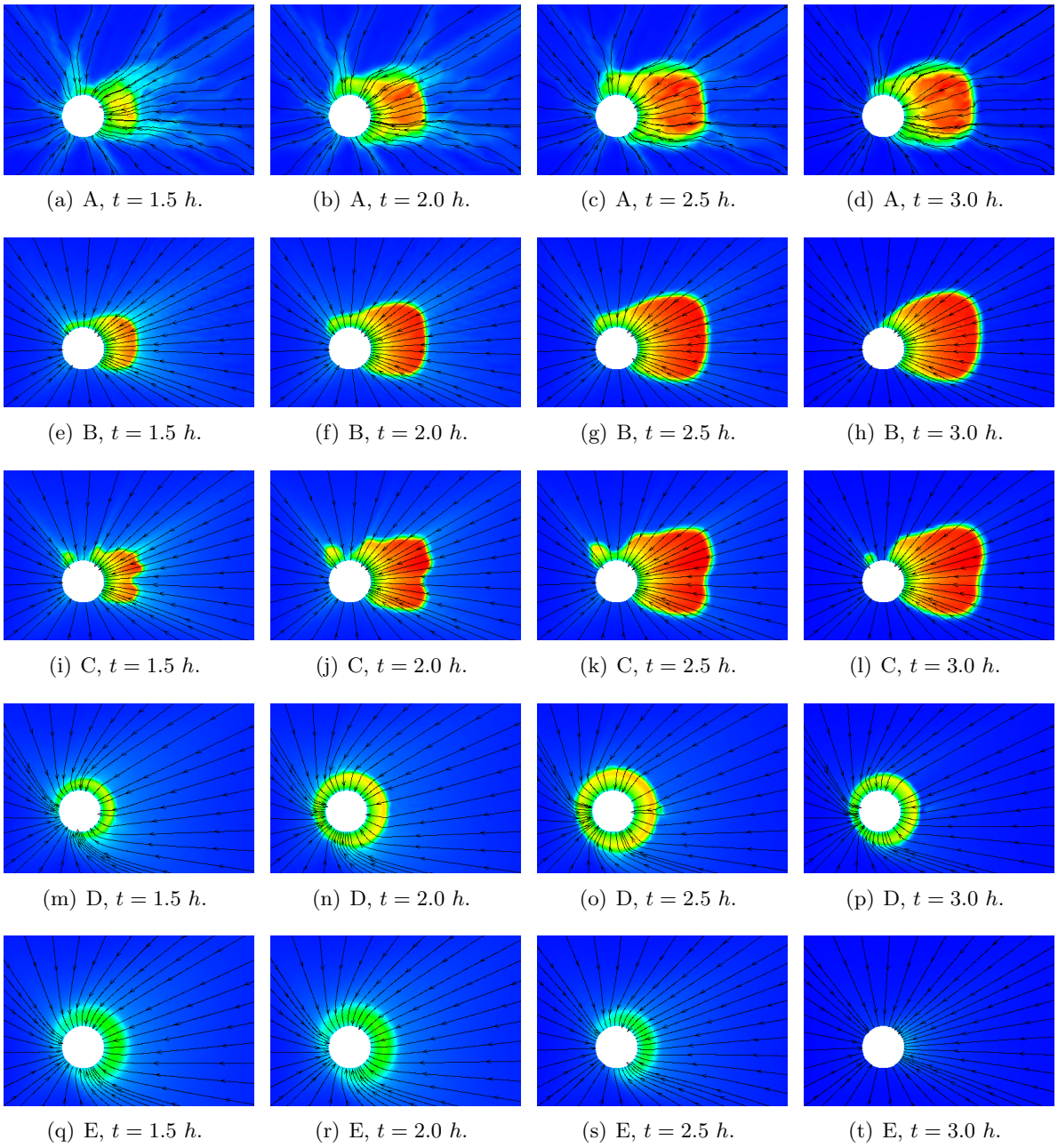

(a) A, $t = 1.5\ h$. (b) A, $t = 2.0\ h$. (c) A, $t = 2.5\ h$. (d) A, $t = 3.0\ h$.

(e) B, $t = 1.5\ h$. (f) B, $t = 2.0\ h$. (g) B, $t = 2.5\ h$. (h) B, $t = 3.0\ h$.

(i) C, $t = 1.5\ h$. (j) C, $t = 2.0\ h$. (k) C, $t = 2.5\ h$. (l) C, $t = 3.0\ h$.

(m) D, $t = 1.5\ h$. (n) D, $t = 2.0\ h$. (o) D, $t = 2.5\ h$. (p) D, $t = 3.0\ h$.

(q) E, $t = 1.5\ h$. (r) E, $t = 2.0\ h$. (s) E, $t = 2.5\ h$. (t) E, $t = 3.0\ h$.

Figure 5.7: **Density and velocity plot comparison at different times.**

Figure 5.7 shows a comparison of the density and flow vector plots for different route-choice strategies at different times. We can see that travelers can make a detour near the high-density regions, except in Strategy C. However, travelers using the local route-choice strategy (Fig. 5.7(a)-(h)) only being to change directions when they obtain density information inside their local perception region. In addition, the paths of travelers using Strategy A are more curved than those using Strategy B, as the former aim to minimize travel time, even if this requires making a detour. In contrast, travelers using Strategy B aim to move closer to the *CBD* within a short time, and therefore do not make many detours. Travelers using Strategy C (Fig. 5.7(i)-(l)) only consider their straight-line distance from the *CBD* and their travel cost is their travel distance, so they always travel straight to the *CBD* without changing direction; thus, the shape of the high-density area is

determined only by the location and shape of the *CBD*. Travelers using strategies D and E (Fig. 5.7(m)-(p)) make the most detours, as global traffic information is available and they can make decisions efficiently. In strategies D and E, travelers from north and south may travel west first to reach the *CBD* without encountering the high-density regions, which makes the distribution of vehicles around the *CBD* more even than in other strategies. The high-density regions in strategies D and E are concentrated near the *CBD* during $t \in [2.0, 2.5]$ h, while in strategies A and B there remains some congestion near the city center at this time. This is clearly shown in Fig. 5.4, in which the outflows of strategies D and E during $t \in [2.0, 2.5]$ h are the highest, followed by those in strategies A and B, and then that of Strategy C.

In addition to the overall traffic situation, the travel of individual vehicles can also be tracked. The tracking method we utilize involves determining the vehicle's position in the next discrete time layer using its current velocity information. This process is repeated in subsequent time layers until the vehicle reaches the Central Business District (CBD) boundary. Without loss of generality, we consider a vehicle departing from location $(15\ km, 12\ km)$ at $t = 1\ h$ as an example. Figure 5.8(a) shows the trajectory comparison and Fig. 5.8(b) shows the total real travel-time comparison. Travelers following strategies A and B can change directions when making route choices. Travelers following Strategy C travel straight toward the *CBD* without considering the traffic dynamics; it is therefore no surprise that although they cover the shortest distance, it takes them the longest time to reach the *CBD*. Travelers following strategies D and E can avoid high-density regions by considering global traffic information. They take a very short time to reach the *CBD*.

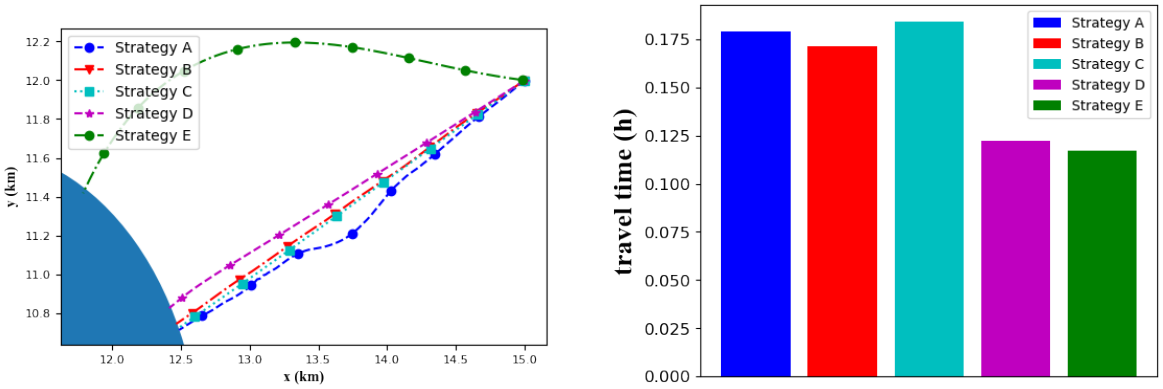

(a) Trajectory (b) Travel time

Figure 5.8: **A typical example demonstrating that global route-choice strategies perform better in most cases.**

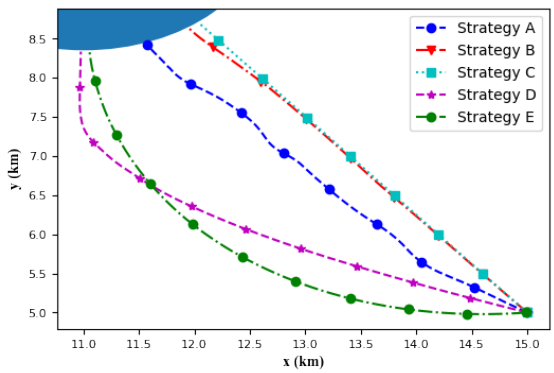

(a) Trajectory from (15 km, 5 km).

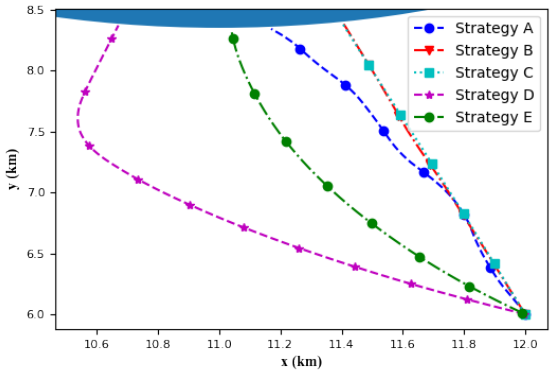

(b) Trajectory from (12 km, 6 km).

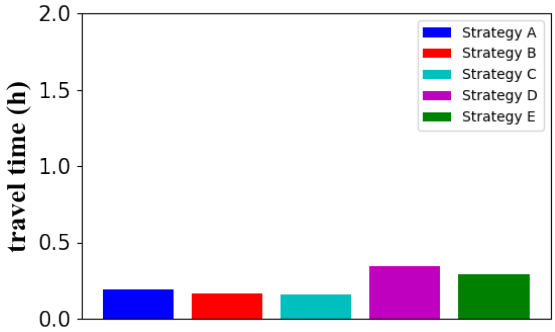

(c) Travel time from (15 km, 5 km).

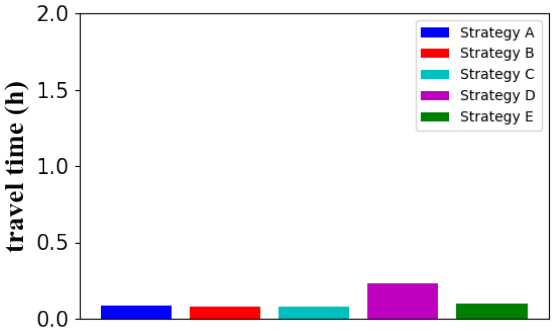

(d) Travel time from (12 km, 6 km).

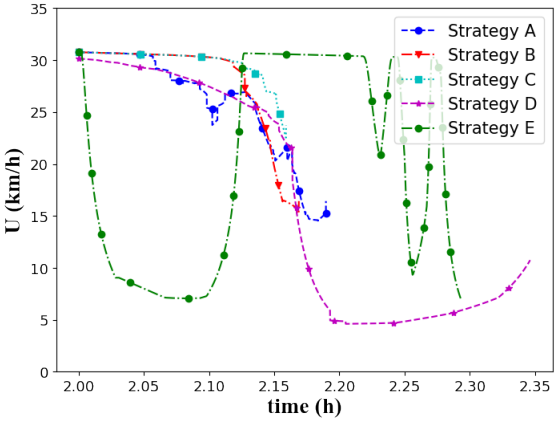

(e) Evolution of speed from (15 km, 5 km).

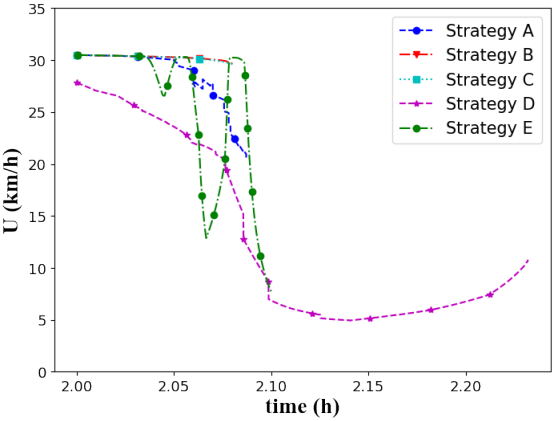

(f) Evolution of speed from (12 km, 6 km).

Figure 5.9: **A rare example illustrating that local route-choice strategies perform better in certain situations.**

Interestingly, global route-choice strategies D and E are not always better than local route-choice strategies A and B for individual travelers: a proportion of travelers using local route-choice strategies take less time to reach the *CBD* than those using global route-choice strategies. The subfigures on the left-hand side and right-hand side of Fig. 5.9 show the traffic information of travelers departing from point (15 km, 5 km) and point (12 km, 6 km) at $t = 2\ h$, respectively. Similar to Fig. 5.8, Fig. 5.9(a)-(b) show that compared to travelers following other strategies, travelers following the global strategy adopt more curved trajectories to avoid the highly congested region. However, Fig. 5.9(c)-(d) show that travelers following strategies A and B arrive at the

CBD earlier than those following strategies D and E, which is in contrast to the observation in 5.8(b). This is probably because in strategies A and B, travelers consider only local information, and thus travelers in different parts of the city have unequal information. Hence, the behaviors of travelers diverge greatly and few individuals reach the *CBD* efficiently, meanwhile, the overall traffic efficiency of the city remains relatively low. In contrast, in global strategies D and E, all travelers obtain the same global traffic information. However, under global user equilibrium principles, individuals do not cooperate and there is thus the potential for competition. Hence, we observe that travelers departing at $t = 2\ h$ from point (15 km, 5 km) and point (12 km, 6 km) following local strategies may reach the *CBD* more efficiently than travelers following global strategies. Nevertheless, by reference to the previous results, we can see that the overall efficiency under global strategies remains significantly enhanced.

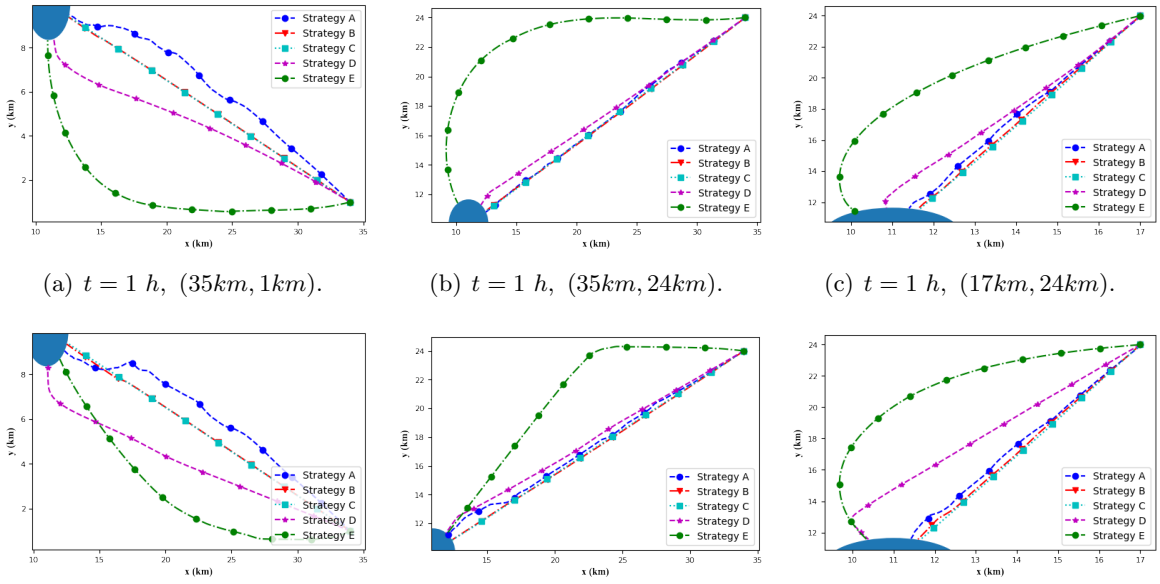

(a) $t = 1\ h,\ (35km, 1km)$. (b) $t = 1\ h,\ (35km, 24km)$. (c) $t = 1\ h,\ (17km, 24km)$.

(d) $t = 2\ h,\ (35km, 1km)$. (e) $t = 2\ h,\ (35km, 24km)$. (f) $t = 2\ h,\ (17km, 24km)$.

Figure 5.10: **Trajectory plots of various vehicles departing from different times and locations.**

Additionally, to provide a more comprehensive illustration, we have included trajectory plots of vehicles departing at $t = 1\ h$ and $t = 2\ h$ from various locations in Fig. 5.10. The titles of the subgraphs indicate the departure times and locations. We can observe that travelers following Strategy A do so more frequently than those following Strategy B. Travelers adhering to Strategies D and E tend to take significant detours to avoid high-density regions, while those following Strategy C consistently travel straight ahead. These observations align with our expectations.

5.2 Example 2: an additional blockage region

5.2.1 Problem Settings

According to the problem settings of Example 1, we consider the case in which a blockage happens near the *CBD* owing to traffic accidents or road breakdowns. As shown by the green circle in Fig. 5.11, the blockage occurs during $t \in (1, 3)\ h$ within a circular region Ω_B with radius 1.5 km. The blockage center is located at $(x_c, y_c) = (15\ km, 10\ km)$. During the blockage, the free-flow

speed U_f within Ω_B is reduced to $0.2U_f$, indicating that some traffic lanes are occupied. After $t = 3$ h, the free-flow speed returns to the normal U_f as defined in Example 1.

5.2.2 Numerical Results

In Figs. 5.12, 5.13 and 5.14, we compare the behaviors of travelers under different strategies. We mark the blockage region Ω_B with a black circle and compare the results of the cases with and without a blockage. For the case in which a blockage occurs during $t \in (1, 3)$ h, travelers under different strategies react differently to the blockage. Travelers under strategies A, B, and C are likely to get stuck within Ω_B, resulting in the expansion of the high-density region behind the blockage area, compared with the blockage-free case. Because travelers move slowly within Ω_B and faster once they drive out of the blockage area, a low-density region occurs between the *CBD* and Ω_B. Compared with Strategy C, travelers under local strategies can change direction to reduce travel cost, and some of them even make a slight detour at the boundary of Ω_B to avoid the blockage area. Travelers under Strategy A (Figs. 5.12d–f) can more easily choose curved routes to avoid the blockage area compared with travelers under Strategy B (Figs. 5.12j–l). Travelers under Strategy C (Figs. 5.13d–f) move straight toward the *CBD*. They neither avoid the blockage area nor optimize their paths when getting stuck in the blockage. Hence, Strategy C features the most congested traffic conditions, both outside and inside the blockage. Under the global route-choice strategies D and E (Figs. 5.13j–l, 5.14d–f), because the global traffic information is available to every driver in the city, travelers can bypass the blockage region Ω_B and reduce overall travel costs.

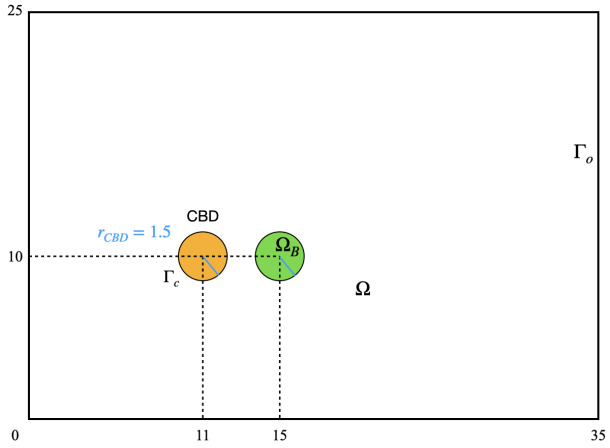

Figure 5.11: **The modeled domain with a blockage region.**

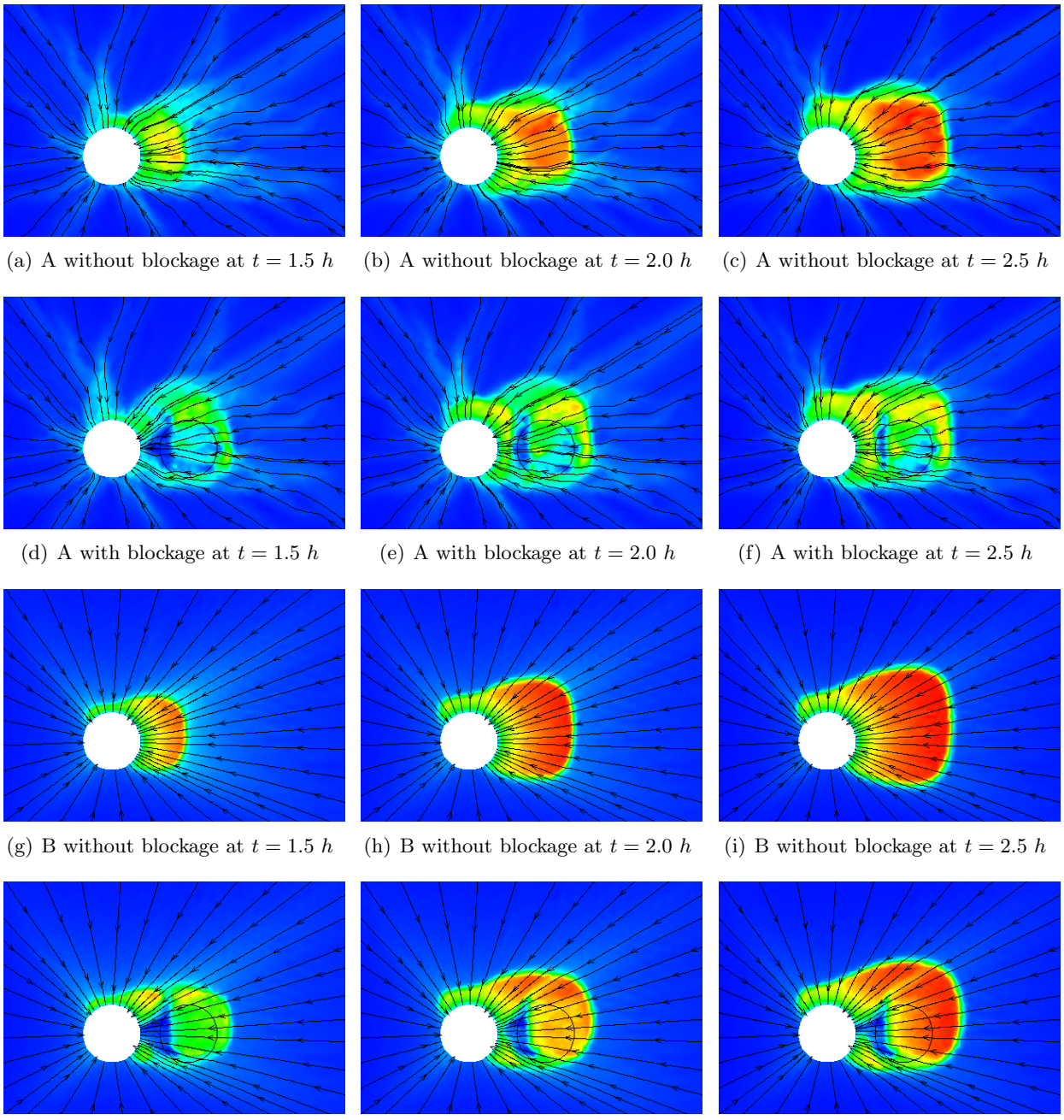

(a) A without blockage at $t = 1.5\ h$ (b) A without blockage at $t = 2.0\ h$ (c) A without blockage at $t = 2.5\ h$

(d) A with blockage at $t = 1.5\ h$ (e) A with blockage at $t = 2.0\ h$ (f) A with blockage at $t = 2.5\ h$

(g) B without blockage at $t = 1.5\ h$ (h) B without blockage at $t = 2.0\ h$ (i) B without blockage at $t = 2.5\ h$

(j) B with blockage at $t = 1.5\ h$ (k) B with blockage at $t = 2.0\ h$ (l) B with blockage at $t = 2.5\ h$

Figure 5.12: **Density and velocity plot comparison without and with blockage - strategies A and B.**

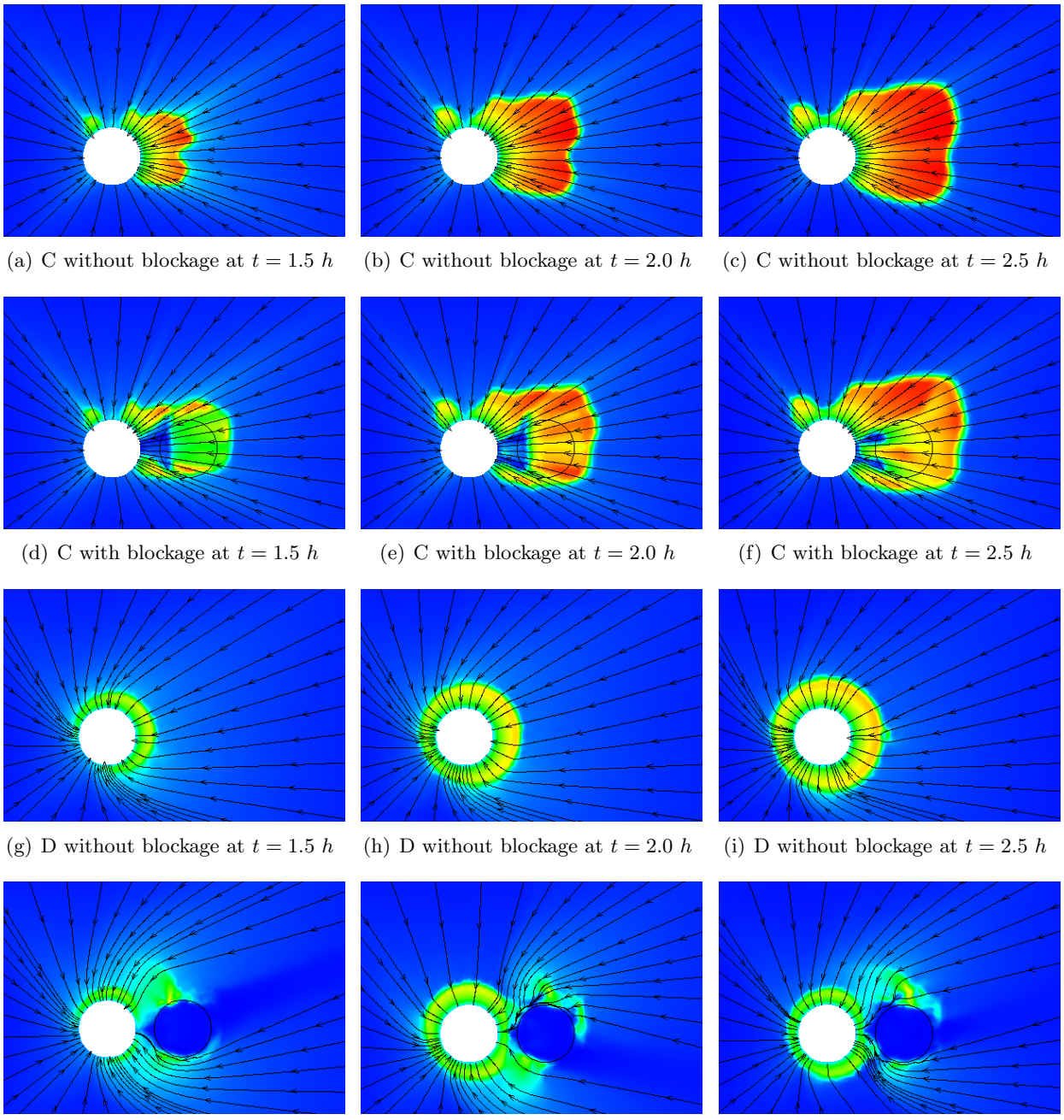

(a) C without blockage at $t = 1.5\ h$ (b) C without blockage at $t = 2.0\ h$ (c) C without blockage at $t = 2.5\ h$

(d) C with blockage at $t = 1.5\ h$ (e) C with blockage at $t = 2.0\ h$ (f) C with blockage at $t = 2.5\ h$

(g) D without blockage at $t = 1.5\ h$ (h) D without blockage at $t = 2.0\ h$ (i) D without blockage at $t = 2.5\ h$

(j) D with blockage at $t = 1.5\ h$ (k) D with blockage at $t = 2.0\ h$ (l) D with blockage at $t = 2.5\ h$

Figure 5.13: **Density and velocity plot comparison without and with blockage - strategies C and D.**

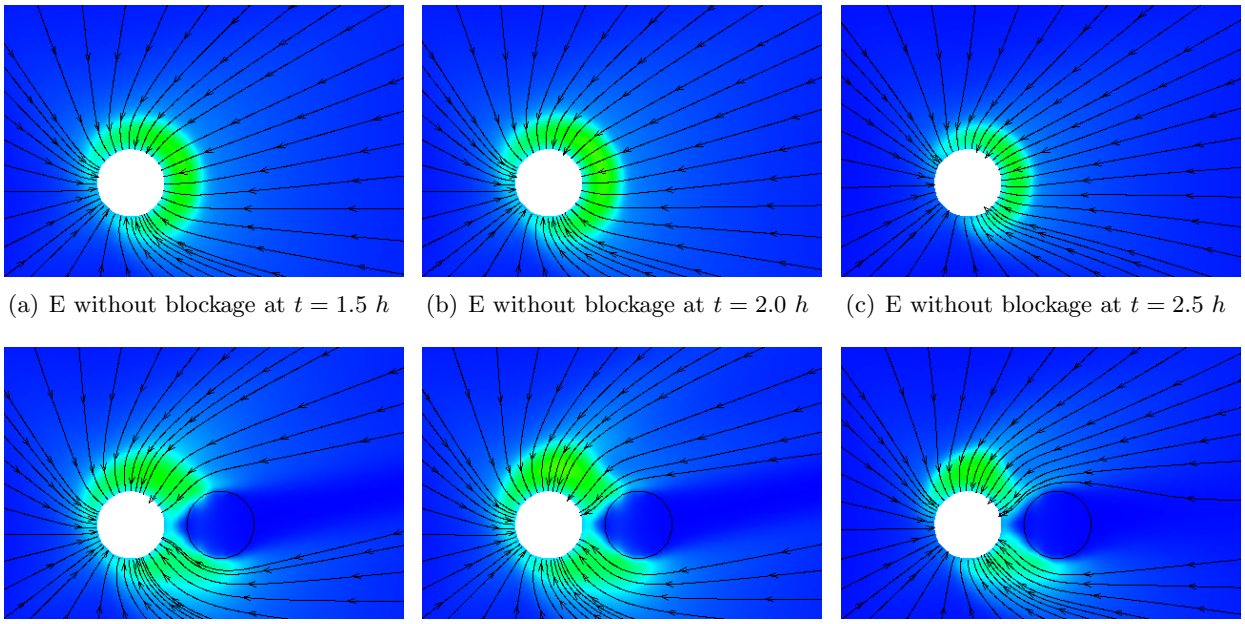

(a) E without blockage at $t = 1.5\ h$ (b) E without blockage at $t = 2.0\ h$ (c) E without blockage at $t = 2.5\ h$

(d) E with blockage at $t = 1.5\ h$ (e) E with blockage at $t = 2.0\ h$ (f) E with blockage at $t = 2.5\ h$

Figure 5.14: **Density and velocity plot comparison without and with blockage - Strategy E.**

For the local strategies A and B, the T_{perc} value reflects the size of the local distance horizon. Figures 5.15 and 5.16 show the performances under different T_{perc} values. With an increased T_{perc} value and hence an enlarged local perception region, travelers can more easily change moving direction and avoid the blockage area, and hence, the local congestion intensity can be reduced, particularly in the peripheral region near the blockage. Moreover, at a small T_{perc}, travelers move in an almost straight line to the *CBD*, and hence, a small congestion region exists on the northwest corner of the *CBD*. With an increased distance horizon, the distribution of vehicles around the *CBD* becomes more even, showing an increased overall traffic efficiency. Strategy A is more sensitive to T_{perc} because travelers make more turns around the blockage. With increasing T_{perc}, travelers under Strategy A are less susceptible to getting stuck in a blockage; therefore, they can more quickly access the *CBD*, reducing the extent of high-density areas.

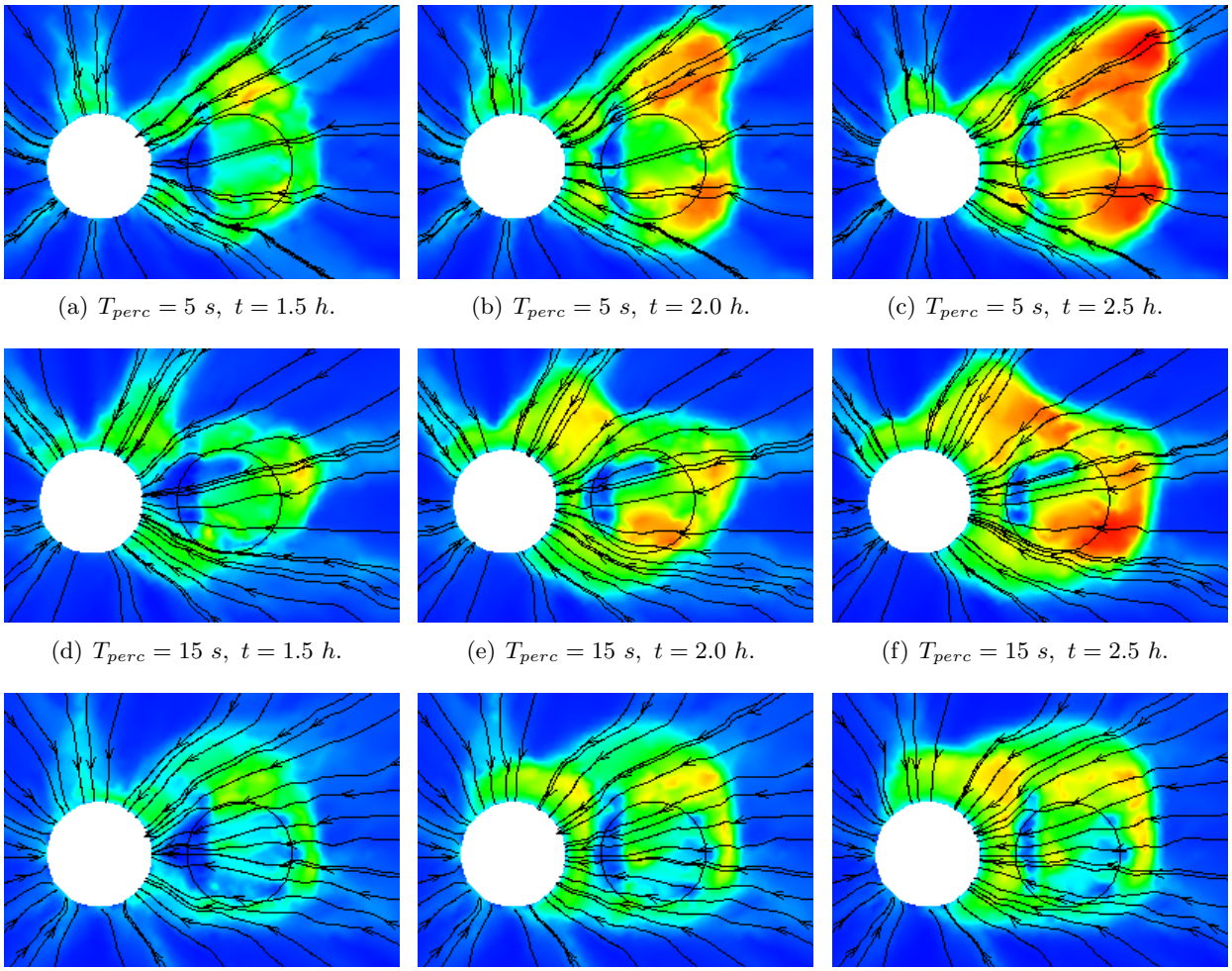

(a) $T_{perc} = 5\ s,\ t = 1.5\ h.$ (b) $T_{perc} = 5\ s,\ t = 2.0\ h.$ (c) $T_{perc} = 5\ s,\ t = 2.5\ h.$

(d) $T_{perc} = 15\ s,\ t = 1.5\ h.$ (e) $T_{perc} = 15\ s,\ t = 2.0\ h.$ (f) $T_{perc} = 15\ s,\ t = 2.5\ h.$

(g) $T_{perc} = 30\ s,\ t = 1.5\ h.$ (h) $T_{perc} = 30\ s,\ t = 2.0\ h.$ (i) $T_{perc} = 30\ s,\ t = 2.5\ h.$

Figure 5.15: **Comparison under different T_{perc} for Strategy A.**

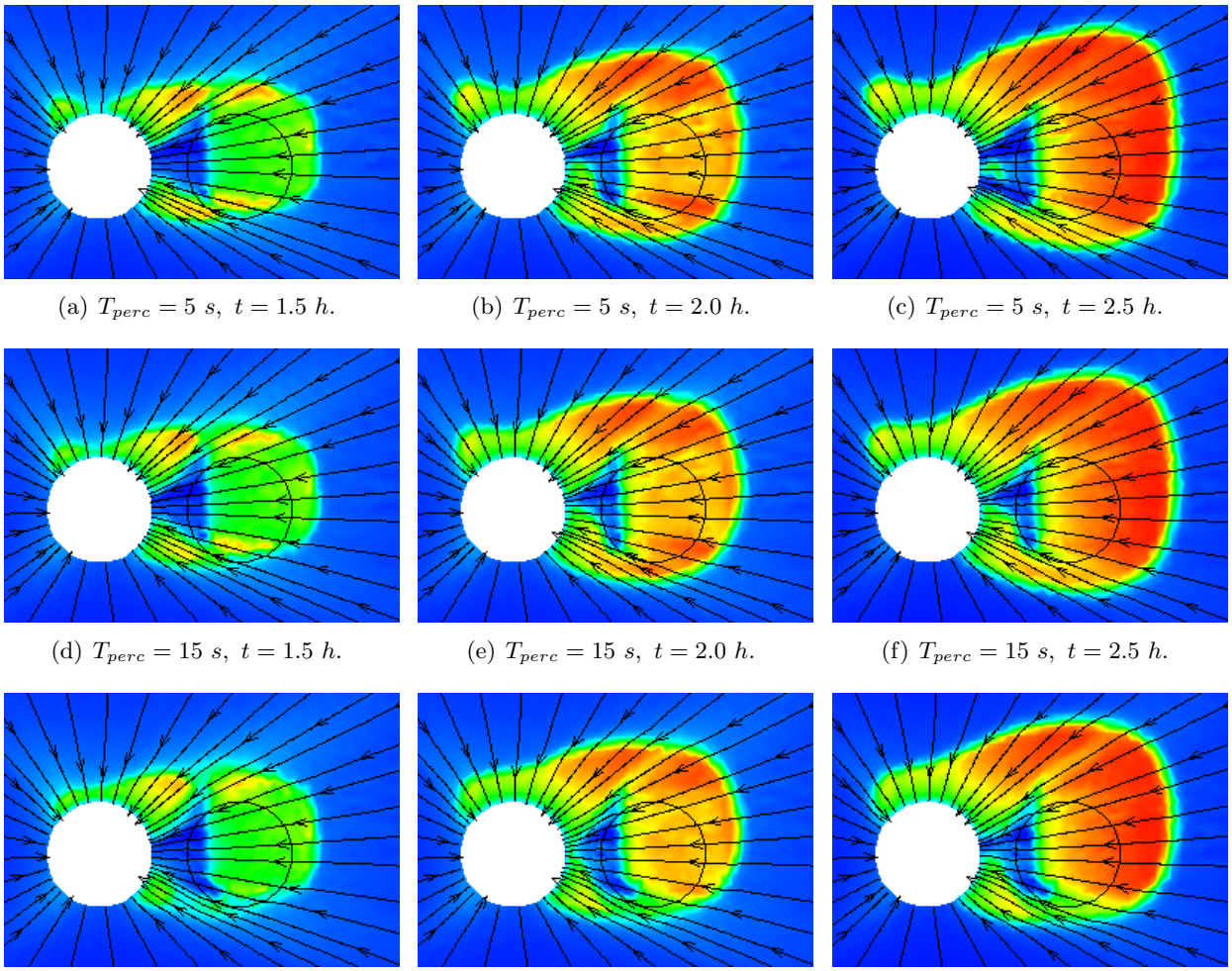

(a) $T_{perc} = 5\ s,\ t = 1.5\ h.$ (b) $T_{perc} = 5\ s,\ t = 2.0\ h.$ (c) $T_{perc} = 5\ s,\ t = 2.5\ h.$

(d) $T_{perc} = 15\ s,\ t = 1.5\ h.$ (e) $T_{perc} = 15\ s,\ t = 2.0\ h.$ (f) $T_{perc} = 15\ s,\ t = 2.5\ h.$

(g) $T_{perc} = 30\ s,\ t = 1.5\ h.$ (h) $T_{perc} = 30\ s,\ t = 2.0\ h.$ (i) $T_{perc} = 30\ s,\ t = 2.5\ h.$

Figure 5.16: **Comparison under different T_{perc} for Strategy B.**

Moreover, Fig. 5.17 presents a comprehensive view of the scenario by displaying trajectories similar to those in Fig. 5.10. The titles of the subgraphs indicate the departure times and locations of certain vehicles. These observations are also in line with our expectations.

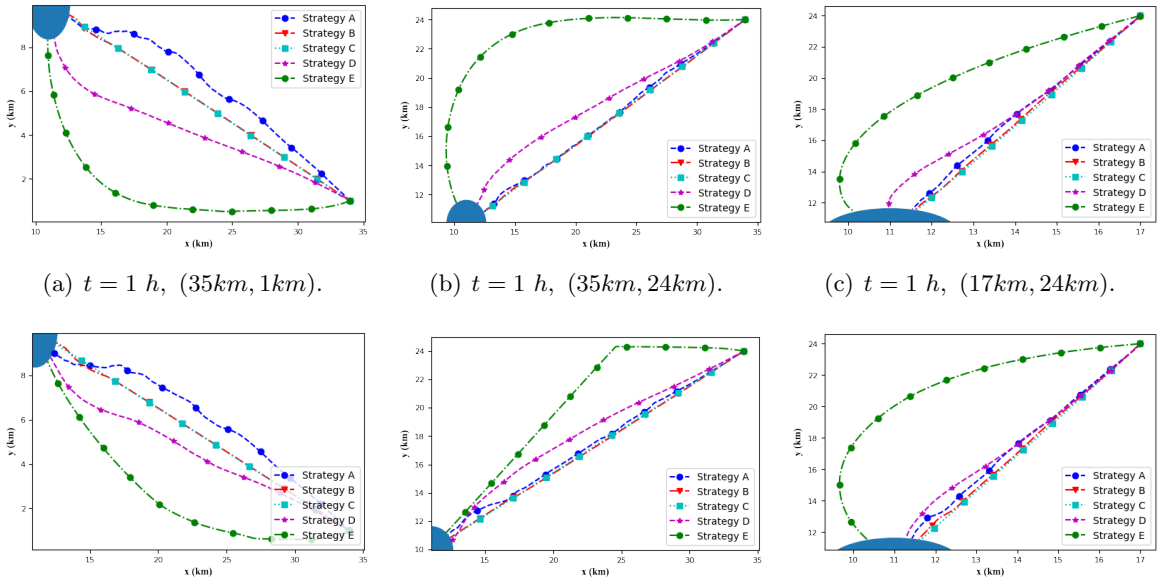

(a) $t = 1\ h,\ (35km, 1km)$. (b) $t = 1\ h,\ (35km, 24km)$. (c) $t = 1\ h,\ (17km, 24km)$.

(d) $t = 2\ h,\ (35km, 1km)$. (e) $t = 2\ h,\ (35km, 24km)$. (f) $t = 2\ h,\ (17km, 24km)$.

Figure 5.17: **Trajectory plots of various vehicles departing at different times and from distinct locations.**

6 Conclusions

In this study, we examine route-choice strategies in DTA problems based on the continuum modeling approach. A two-dimensional city with a single *CBD* is considered. Most existing models assume that travelers have a global perception of traffic dynamics across an entire city. In contrast, we also study the behavior of travelers who have only a local view of a city and thus we consider local route-choice strategies. We assume that travelers can only obtain dynamic traffic information for a small local area. We devise two new local route-choice strategies, denoted strategies A and B. The complete model for Strategy A includes a local potential function solved by an eikonal equation within a local feasible region, whereas the complete model for Strategy B includes a minimum value problem equipped with ODEs. Both models include a conservation law to obtain the density and determine the traffic flow level.

To demonstrate the effectiveness of these models, we use numerical examples and compare various route-choice strategies using unstructured mesh grids and also consider a case with blockage inside the city. The numerical results are in line with our expectations. We find that a higher traveling efficiency is obtained as the local perception of traffic dynamics improves, and that the city's overall traffic efficiency in local route-choice strategies is higher than that in a strategy with no real-time traffic information and lower than that in a global route-choice strategy with instantaneous or actual traffic information. Nevertheless, some individual vehicles travel faster in local route-choice strategies than in global route-choice strategies. This may be because RDUE and PDUE models are not DSO. Although there is global information, all travelers possess it, so there is competition between them until equilibrium is achieved. Thus, from an individual traveler's point of view, a local strategy is sometimes better than a global strategy.

We analyze several possible route-choice strategies separately. In future studies, we will consider mixed traffic flow models, such as a mixture of cooperative autonomous vehicles and human vehicles, and develop a traffic model with various mixed route-choice strategies. Moreover, in future work,

T_{perc} could be varied for different parts of the city Ω. Although we cannot specify a particular vehicle type, we can change the size of the perception region in the city, which is determined by the city's spatial structure. In addition, although we use a continuous traffic flow model in which the roads are so dense that it is almost impossible to consider vehicles as moving freely in the city, the shape and range of the perception region can nevertheless differ from the actual traffic distribution in the city, which corresponds to the local region $\Omega_{(x,y,t)}$ in Strategy A. For example, the width of an intersection determines the range of perception of vehicles at that location. Finally, for the sake of simplicity, this study focuses only on deterministic route choices; in future, we will also study choices of departure time.

As our aim is to compare various route-choice strategies, we only solve a simple numerical example. However, our model is also applicable to a situation with multiple *CBD*s and multiple obstructed areas (such as those occupied by lakes). In future work, we will also study multiple groups of traffic units in a city, as route-choice strategies may vary between groups. Furthermore, although we study traffic flow with our model, it is also widely applicable to other similar traffic scenarios, such as pedestrian flow on a platform and the emergency evacuation of crowds in shopping malls, and thus provides a good reference for setting macro-level guidance for such situations.

Acknowledgments

This work was jointly supported by grants from the National Key R&D Program of China (Grant No. 2021YFA0719200), the Key Program of the National Natural Science Foundation of China (Grant No. U21B2089), and the Research Grants Council of the Hong Kong Special Administrative Region, China (Project No. 17202223). The last author was also supported by the Francis S Y Bong Professorship in Engineering.

Reference

[1] S. Bekhor, M. E. Ben-Akiva, and M. S. Ramming. Evaluation of choice set generation algorithms for route choice models. *Annals of Operations Research*, 144(1):235–247, 2006.

[2] D. E. Boyce, B. Ran, and L. J. Leblanc. Solving an instantaneous dynamic user-optimal route choice model. *Transportation Science*, 29(2):128–142, 1995.

[3] D. Buckley. Traffic assignment in a two-dimensional continuous representation of a traffic network with flow-dependent speeds. *Transportation Research Part B: Methodological*, 13(2):167–179, 1979.

[4] A. H. F. Chow. Dynamic system optimal traffic assignment–a state-dependent control theoretic approach. *Transportmetrica*, 5(2):85–106, 2009.

[5] B. Cockburn, S. Hou, and C.-W. Shu. The Runge-Kutta local projection discontinuous Galerkin finite element method for conservation laws. IV. The multidimensional case. *Mathematics of Computation*, 54(190):545–581, 1990.

[6] B. Cockburn, S.-Y. Lin, and C.-W. Shu. TVB Runge-Kutta local projection discontinuous Galerkin finite element method for conservation laws III: one-dimensional systems. *Journal of computational Physics*, 84(1):90–113, 1989.

[7] B. Cockburn and C.-W. Shu. TVB Runge-Kutta local projection discontinuous Galerkin finite element method for conservation laws. II. general framework. *Mathematics of computation*, 52(186):411–435, 1989.

[8] B. Cockburn and C.-W. Shu. The Runge-Kutta local projection-discontinuous-Galerkin finite element method for scalar conservation laws. *ESAIM: Mathematical Modelling and Numerical Analysis*, 25(3):337–361, 1991.

[9] B. Cockburn and C.-W. Shu. The Runge-Kutta discontinuous Galerkin method for conservation laws V: multidimensional systems. *Journal of Computational Physics*, 141(2):199–224, 1998.

[10] J. Conlisk. Why bounded rationality? *Journal of economic literature*, 34(2):669–700, 1996.

[11] J. Del Castillo and F. Benitez. On the functional form of the speed-density relationship—II: empirical investigation. *Transportation Research Part B: Methodological*, 29(5):391–406, 1995.

[12] X. Di and H. X. Liu. Boundedly rational route choice behavior: A review of models and methodologies. *Transportation Research Part B: Methodological*, 85:142–179, 2016.

[13] J. Du, S. C. Wong, C.-W. Shu, T. Xiong, M. Zhang, and K. Choi. Revisiting Jiang's dynamic continuum model for urban cities. *Transportation Research Part B: Methodological*, 56:96–119, 2013.

[14] J. Du, S. C. Wong, C.-W. Shu, and M. Zhang. Reformulating the Hoogendoorn-Bovy predictive dynamic user-optimal model in continuum space with anisotropic condition. *Transportation Research Part B: Methodological*, 79:189–217, 2015.

[15] R.-Y. Guo and H.-J. Huang. Logit-based exit choice model of evacuation in rooms with internal obstacles and multiple exits. *Chinese Physics B*, 19(3):030501, 2010.

[16] A. Haurie and P. Marcotte. On the relationship between Nash—Cournot and Wardrop equilibria. *Networks*, 15(3):295–308, 1985.

[17] S. P. Hoogendoorn and P. H. Bovy. Dynamic user-optimal assignment in continuous time and space. *Transportation Research Part B: Methodological*, 38(7):571–592, 2004.

[18] S. P. Hoogendoorn and P. H. Bovy. Pedestrian route-choice and activity scheduling theory and models. *Transportation Research Part B: Methodological*, 38(2):169–190, 2004.

[19] S. P. Hoogendoorn, F. van Wageningen-Kessels, W. Daamen, D. C. Duives, and M. Sarvi. Continuum theory for pedestrian traffic flow: Local route choice modelling and its implications. *Transportation Research Part C: Emerging Technologies*, 59:183–197, 2015. Special Issue on International Symposium on Transportation and Traffic Theory.

[20] H.-J. Huang and W. H. Lam. Modeling and solving the dynamic user equilibrium route and departure time choice problem in network with queues. *Transportation Research Part B: Methodological*, 36(3):253–273, 2002.

[21] L. Huang, S. C. Wong, M. Zhang, C.-W. Shu, and W. H. K. Lam. Revisiting Hughes' dynamic continuum model for pedestrian flow and the development of an efficient solution algorithm. *Transportation Research Part B: Methodological*, 43(1):127–141, 2009.

[22] G.-S. Jiang and C.-W. Shu. Efficient implementation of weighted ENO schemes. *Journal of computational physics*, 126(1):202–228, 1996.

[23] L. Krivodonova, J. Xin, J.-F. Remacle, N. Chevaugeon, and J. E. Flaherty. Shock detection and limiting with discontinuous Galerkin methods for hyperbolic conservation laws. *Applied Numerical Mathematics*, 48(3-4):323–338, 2004.

[24] M. Kuwahara and T. Akamatsu. Dynamic user optimal assignment with physical queues for a many-to-many OD pattern. *Transportation Research Part B: Methodological*, 35(5):461–479, 2001.

[25] P. D. Lax. Weak solutions of nonlinear hyperbolic equations and their numerical computation. *Communications on Pure and Applied Mathematics*, 7(1):159–193, 1954.

[26] M. J. Lighthill and G. B. Whitham. On kinematic waves II. A theory of traffic flow on long crowded roads. *Proceedings of the Royal Society of London. Series A. Mathematical and Physical Sciences*, 229(1178):317–345, 1955.

[27] H. K. Lo and W. Y. Szeto. A cell-based dynamic traffic assignment model: formulation and properties. *Mathematical and Computer Modelling*, 35(7-8):849–865, 2002.

[28] H. K. Lo and W. Y. Szeto. A cell-based variational inequality formulation of the dynamic user optimal assignment problem. *Transportation Research Part B: Methodological*, 36(5):421–443, 2002.

[29] H. K. Lo and W. Y. Szeto. Road pricing modeling for hyper-congestion. *Transportation Research Part A: Policy and Practice*, 39(7-9):705–722, 2005.

[30] J. Long, W. Y. Szeto, J. Du, and R. C. P. Wong. A dynamic taxi traffic assignment model: A two-level continuum transportation system approach. *Transportation Research Part B: Methodological*, 100:222–254, 2017.

[31] T. Lotan. Effects of familiarity on route choice behavior in the presence of information. *Transportation Research Part C: Emerging Technologies*, 5(3-4):225–243, 1997.

[32] D. K. Merchant and G. L. Nemhauser. A model and an algorithm for the dynamic traffic assignment problems. *Transportation Science*, 12(3):183–199, 1978.

[33] D. K. Merchant and G. L. Nemhauser. Optimality conditions for a dynamic traffic assignment model. *Transportation Science*, 12(3):200–207, 1978.

[34] G. F. Newell. Nonlinear effects in the dynamics of car following. *Operations research*, 9(2):209–229, 1961.

[35] J. Qian, Y.-T. Zhang, and H.-K. Zhao. Fast sweeping methods for eikonal equations on triangular meshes. *SIAM Journal on Numerical Analysis*, 45(1):83–107, 2007.

[36] Z. S. Qian and H. M. Zhang. A hybrid route choice model for dynamic traffic assignment. *Networks and Spatial Economics*, 13(2):183–203, 2013.

[37] M. S. Ramming. Network knowledge and route choice. *Ph. D. Thesis, Massachusetts Institute of Technology*, 2001.

[38] B. Ran and D. Boyce. *Modeling dynamic transportation networks: an intelligent transportation system oriented approach*. Springer Berlin Heidelberg, 1996.

[39] P. I. Richards. Shock waves on the highway. *Operations Research*, 4(1):42–51, 1956.

[40] C.-W. Shu and S. Osher. Efficient implementation of essentially non-oscillatory shock-capturing schemes. *Journal of computational physics*, 77(2):439–471, 1988.

[41] W. Y. Szeto and H. K. Lo. Dynamic traffic assignment: review and future research directions. *Journal of Transportation Systems Engineering and Information Technologiy,(5)*, pages 85–100, 2005.

[42] K. van der El, D. M. Pool, M. M. van Paassen, and M. Mulder. Modeling driver steering behavior in restricted-preview boundary-avoidance tasks. *Transportation Research Part F: Traffic Psychology and Behaviour*, 94:362–378, 2023.

[43] K. van der El, D. M. Pool, M. R. M. van Paassen, and M. Mulder. A unifying theory of driver perception and steering control on straight and winding roads. *IEEE Transactions on Human-Machine Systems*, 50(2):165–175, 2020.

[44] R. Vaughan. *Urban spatial traffic patterns*. Pion Limited, England, 1987.

[45] E. I. Vlahogianni, M. G. Karlaftis, and J. C. Golias. Short-term traffic forecasting: where we are and where we're going. *Transportation Research Part C: Emerging Technologies*, 43:3–19, 2014.

[46] W. L. Wang, S. M. Lo, and S. B. Liu. A cognitive pedestrian behavior model for exploratory navigation: visibility graph based heuristics approach. *Simulation Modelling Practice and Theory*, 77:350–366, 2017.

[47] J. G. Wardrop. Road paper. Some theoretical aspects of road traffic research. *Proceedings of the Institution of Civil Engineers*, 1(3):325–362, 1952.

[48] S. C. Wong. Multi-commodity traffic assignment by continuum approximation of network flow with variable demand. *Transportation Research Part B: Methodological*, 32(8):567–581, 1998.

[49] S. C. Wong, C. K. Lee, and C. O. Tong. Finite element solution for the continuum traffic equilibrium problems. *International Journal for Numerical Methods in Engineering*, 43(7):1253–1273, 1998.

[50] Y. Xia, S. Wong, M. Zhang, C.-W. Shu, and W. H. Lam. An efficient discontinuous Galerkin method on triangular meshes for a pedestrian flow model. *International Journal for Numerical Methods in Engineering*, 76(3):337–350, 2008.

[51] Y. Xia, S. C. Wong, and C.-W. Shu. Dynamic continuum pedestrian flow model with memory effect. *Physical Review E*, 79(6):066113, 2009.

[52] L. Yang, T. Li, S. C. Wong, C.-W. Shu, and M. Zhang. Modeling and simulation of urban air pollution from the dispersion of vehicle exhaust: A continuum modeling approach. *International Journal of Sustainable Transportation*, 13(10):722–740, 2019.

[53] J.-B. Zeng, B. Leng, and Z. Xiong. Pedestrian dynamics in a two-dimensional complex scenario using a local view floor field model. *International Journal of Modern Physics C - IJMPC*, 22:775–803, 08 2011.

[54] X. Zhang, H.-J. Huang, and H. Zhang. Integrated daily commuting patterns and optimal road tolls and parking fees in a linear city. *Transportation Research Part B: Methodological*, 42(1):38–56, 2008.

[55] X. Zhang, Y. Xia, and C.-W. Shu. Maximum-principle-satisfying and positivity-preserving high order discontinuous Galerkin schemes for conservation laws on triangular meshes. *Journal of Scientific Computing*, 50(1):29–62, 2012.

[56] Y.-T. Zhang, H.-K. Zhao, and J. Qian. High order fast sweeping methods for static Hamilton-Jacobi equations. *Journal of Scientific Computing*, 29(1):25–56, 2006.

[57] X. Zhong and C.-W. Shu. A simple weighted essentially nonoscillatory limiter for Runge-Kutta discontinuous Galerkin methods. *Journal of Computational Physics*, 232(1):397–415, 2013.

[58] Z.-X. Zhou, W. Nakanishi, and Y. Asakura. Route choice in the pedestrian evacuation: Microscopic formulation based on visual information. *Physica A: Statistical Mechanics and its Applications*, 562:125313, 2021.

[59] J. Zhu and J. Qiu. A new fifth order finite difference WENO scheme for solving hyperbolic conservation laws. *Journal of Computational Physics*, 318:110–121, 2016.

[60] J. Zhu, J. Qiu, C.-W. Shu, and M. Dumbser. Runge-Kutta discontinuous Galerkin method using weno limiters II: unstructured meshes. *Journal of Computational Physics*, 227(9):4330–4353, 2008.